Supplementary Information

De Novo Zwitterionic Strategy of Ultra-stable Chemiluminescent Probes: Highly Selective Sensing Singlet Oxygen in FDA-approved Phototherapy

Yao Lu,[‡a] Yutao Zhang,[‡a] Xia Wu,[b] Ruihua Pu,[c] Chenxu Yan,[a] Weimin Liu,[c] Xiaogang Liu,[b] Zhiqian Guo*[a] and Wei-Hong Zhu[a]

[a] Key Laboratory for Advanced Materials and Institute of Fine Chemicals, Feringa Nobel Prize Scientist Joint Research Center, Frontiers Science Center for Materiobiology and Dynamic Chemistry, School of Chemistry and Molecular Engineering, East China University of Science and Technology, Shanghai 200237, China

[b] Fluorescence Research Group, Singapore University of Technology and Design, 8 Somapah Road, Singapore, 487372, Singapore

[c] School of Physical Science and Technology, ShanghaiTech University, Shanghai 201210, China

* Email: guozq@ecust.edu.cn

[‡] These authors contributed equally to this work.

Contents

1. Experimental Section

Materials and General Methods

Unless special stated, all solvents and chemicals were purchased from commercial suppliers in analytical grade and used without further purification. The ^{1}H and ^{13}C NMR spectra were recorded on a Bruker AM 400 spectrometer, using TMS as an internal standard. High-resolution mass spectrometry data were obtained with a Waters LCT Premier XE spectrometer. Absorption spectra were collected on a Varian Cary 500 spectrophotometer, and fluorescence spectra measurements were performed on a Varian Cary Eclipse fluorescence spectrophotometer. The LED white light was purchased from Lasever Inc (LSR-PS-II, 0-1000 mW). We also used the optical power meter to carefully measure the average light intensity (120 mW cm^{-2}) in our experimental conditions. The light power density of lasers used was 200 mW cm^{-2}, which is considered safe for humans in the PDT process. The white light source (PLS-SXE300/300UV) used in photostability experiments was purchased from Beijing Perfectlight Technology Co., Ltd. Chemiluminescence signals in 96-well plates were recorded using an ImageQuant LAS4000 system (GE Healthcare). Each well intensity of 96-well plates was quantified using the ImageQuant TL software (GE Healthcare). Femtosecond transient absorption (TA) spectra were collected using a commercial femtosecond transient absorption spectrometer (Helios fire, Ultrafast System). Confocal fluorescence images were taken on a Leica TCS SP8 (63 × oil lens). Chemiluminescence spectra, *in vivo* chemiluminescence and fluorescence images were measured with a PerkinElmer IVIS Spectrum Imaging System.

Determination of Chemiluminescence

QMI solution (50 μM, including 20 eq Tributylhexadecylphosphonium bromide [TBHP]) in PBS (10 mM, pH 7.4) was placed into the wells of a black 96-well plate, and the different concentrations of photosensitizers (MB, RB, ICG, Cy5 and porphyrins) were added. Chemiluminescence intensities were immediately measured after irradiation using an ImageQuant LAS4000 system (acquisition time of 1 min).

QMI and reference compounds (QMCL, PyCL, and InCL) solutions (50 μM, including 20 eq TBHP) in PBS (10 mM, pH 7.4) were placed into the wells of a black 96-well plate without photosensitizers. Chemiluminescence intensities were immediately measured after irradiation (white LED) using an ImageQuant LAS4000 system (acquisition time of 1 min).

QMI solution (50 μM, including 20 eq TBHP and 10 μM MB) in PBS (10 mM, pH 7.4) was placed into the wells of a black 96-well plate. Chemiluminescence intensities were continuously acquired after irradiation (200 mW cm^{-2} 690 nm laser) using an ImageQuant LAS4000 system (acquisition time of 1 min). The chemiluminescence intensities were plotted as a function of time.

pK_a Determination

The pK_a value of the probe QMI was determined using the Henderson-Hasselbalch equation:

$$\log[(A_{max}-A)/(A-A_{min})] = pK_a-pH$$

where A_{max} and A_{min} represent maximum absorbance and minimal absorbance at the measured wavelength, respectively. A represents the

observed absorbance. The pK_a value was calculated based on the plot of $\log[(A_{max}-A)/(A-A_{min})]$ versus pH.[1]

Photostability Experiment

QMI solution (1 mM) in a mixture of PBS/DMSO (v/v = 1/1) was exposed to white light (1.6 W cm^{-2}) while pumping oxygen into the solution. Samples were taken at 3 min intervals during the light period for high-performance liquid chromatography (HPLC) analysis. High resolution mass spectrometry (HRMS) confirmed the identity of the decomposed fragments. DCMCL and QMCL were tested in the same way.

Cell Experiment

Cell Lines

The human epithelioid cervical carcinoma cell line HeLa was purchased from the Institute of Cell Biology (Shanghai, China). Cells were all propagated in T-75 flasks cultured at 37 ^oC under a humidified 5% CO_2 atmosphere in RPMI-1640 medium or DMEM medium (GIBCO/Invitrogen, Camarillo, CA, USA), which were supplemented with 10 % fetal bovine serum (FBS, Biological Industry, Kibbutz Beit Haemek, Israel) and 1 % penicillin-streptomycin (10,000 U mL^{-1} penicillin and 10 mg/ml streptomycin, Solarbio life science, Beijing, China).

In Vitro Cytotoxicity Assay

The cell cytotoxicity of QMI to HeLa cells was measured by 3-(4, 5-dimethylthiazol-2-yl)-2, 5-diphenyltetrazolium bromide (MTT) assay. The cytotoxicity was evaluated by Cell Counting Kit-8 (Dojindo, Tokyo, Japan) according to the factory's instruction. Cells were plated in 96-well plates in 0.1 mL volume of DMEM or RPMI-1640 medium with 10 % FBS, at a density of 1×10^4 cells/well and added with desired concentrations of QMI. After incubation for 24 h, absorbance was measured at 540 nm with a Tecan GENios Pro multifunction reader (Tecan Group Ltd., Maennedorf, Switzerland). Each concentration was measured in triplicate and used in three independent experiments. The relative cell viability was calculated by the equation: cell viability (%) = $(OD_{treated}/OD_{control}) \times 100\%$.

In Vitro Cellular Fluorescence Imaging

The HeLa cells at 1×10^5 cells/well were seeded onto glass-bottom petri dishes with complete medium (1.5 mL) for 12 h. The cells pro-incubated with 10 μM QMI for 1 h, 20 μM HMME for 2 h or 1 mM 5-ALA for 24 h, respectively. PBS (pH 7.4) was used to wash cells for three times to clean the background. The images were then photographed by using a confocal laser scanning microscope Leica TCS SP8 (63 × oil lens) with 520 nm (group QMI) and 410 nm (group HMME or group 5-ALA) as the excitation wavelength and 600-700 nm (group QMI) and 620-710 nm (group HMME or group 5-ALA) as the emission wavelength.

In Vitro Cellular Chemiluminescence Imaging in 96-Well Plates

The HeLa cells at 1×10^5 cells/well were placed into the wells of a black 96-well plate with complete medium (100 μL) for 12 h. The cells pro-incubated with QMI (20 μM) for 1 h, HMME (20 μM) for 2 h, or HMME followed by QMI for 1 h, respectively. The cells pro-incubated

with QMI (20 μM) for 1 h, 5-ALA (1 mM) for 24 h, or 5-ALA followed by QMI for 1 h, respectively. Cells were washed with PBS (pH 7.4) for 3 times and immediately imaged with or without irradiation (3 min, 635 nm laser) using an ImageQuant LAS4000 system (acquisition time of 5 min).

Animals Experiment

Animals

The mouse experiment procedures and protocols had been approved by the East China University of Science and Technology Animal Studies Committee (ECUST-2021-07001). The 4-week-old female BALB/c nude mice were produced from Shanghai Meixuan Biological Technology Co., Ltd., and maintained under standard conditions. The animals were housed in sterile cages within laminar airflow hoods in a specific pathogen-free room with a 12-h light/12-h dark schedule and fed autoclaved chow and water ad libitum.

In Vivo Chemiluminescence Imaging Experiment

The nude mice were inoculated with HeLa cells on their right flanks by injecting 10^6 cells subcutaneously. When the tumors grew up to 5 mm in diameter, QMI solutions (20 μL) with or without photosensitizers (RB, 10 μM; ICG, 40 μM; or Cy5, 40 μM) were injected into the tumor of mice. Similarly, QMCL, CL-SO or SOSG solution (20 μL) with or without RB (10 μM) was injected into the tumor of mice. The 5-ALA was administered to the mice at a dose of 20 mg/kg via intratumoral injection to construct mice models, then QMI solution (20 μL) was injected into the tumor of mice after 6 hours. The probes concentration of the injected solution was 1×10^{-4} mol L^{-1} (PBS, pH = 7.4, with 1 mM TBHP). *In vivo* chemiluminescence images were acquired under bioluminescence mode (PerkinElmer IVIS Spectrum Imaging System) with an open filter and an acquisition time of 1 min (Control group without additional irradiation).

Computational Details

The density functional theory (DFT) and time-dependent (TD-DFT) were carried out using Gaussian 16A.[2] Geometry optimizations were carried out at the CAM-B3LYP/Def2svp level.[3] Frequency calculations were performed to confirm that we obtained stable structures without imaginary vibration frequencies in the ground and the intramolecular charge transfer states. Solvation effects were taken into account using the SMD model.[4] The excitation energies and emission energies of all molecules were calculated using the corrected linear response (cLR) solvent formalism.

We also constructed the potential energy surfaces of both the S_0 and S_1 states, following the twisted intramolecular charge transfer (TICT) model.[5] We used water as the solvent. During the optimizations of these molecular structures in the S_1 state, two dihedral angles (around θ) were fixed at various values from 0 to 90° at a step size of 10°. The energy levels of the S_0 potential energy surface were retrieved based on optimized structures in the excited state (S_1). The molecular excitation properties were also investigated by the hole-electron analysis using Multiwfn 3.6.[6]

2. Synthetic Method

Compound 1, **DCMCL**, **QMCL** and **CL-SO** were synthesized by the established procedures.[5, 7]

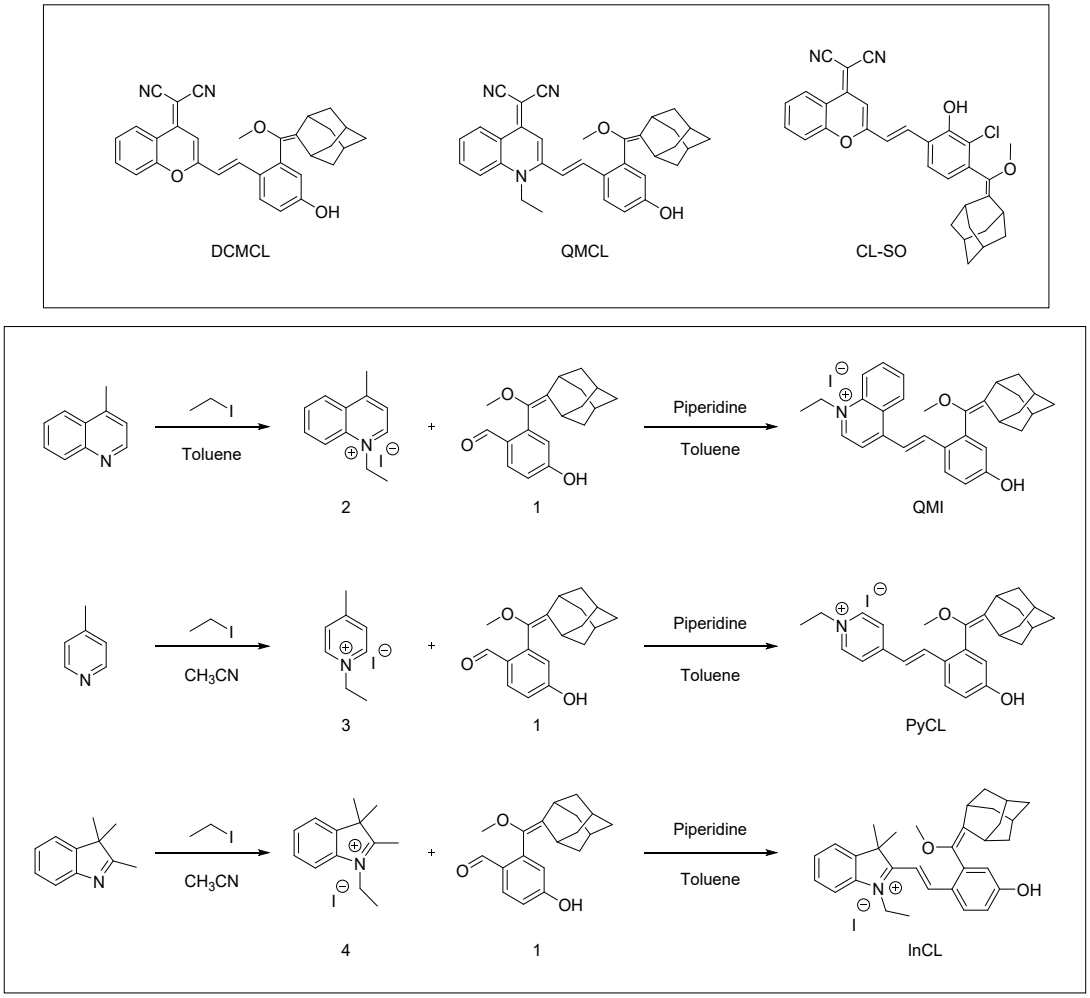

Scheme S1. Synthetic route of **QMI**, **PyCL** and **InCL**

Synthesis of compound 2

4-methylquinoline (1.00 g, 7.00 mmol) and iodoethane (1.68 mL, 21.00 mmol) were dissolved in toluene (2.5 mL). The mixture was under argon protection and then refluxed for 8 h. After cooling to room temperature, the resultant precipitant was collected by filtration and washed with ethyl ether. The solid product was dried in vacuum to afford **compound 2** as a yellow solid (1.97 g): Yield 94%. ^{1}H NMR (400 MHz, $CDCl_3$, ppm): δ 1.81 (t, J = 7.6 Hz, 3H, $NCH_2\boldsymbol{CH_3}$), 3.02 (s, 3H, pyridine-$\boldsymbol{CH_3}$), 5.38 (q, J = 7.2 Hz, 2H, $N\boldsymbol{CH_2}CH_3$), 7.98-8.03 (m, 2H, phenyl-H), 8.19-8.24 (m, 1H, phenyl-H), 8.36-8.41 (m, 2H, phenyl-H), 10.31 (d, J = 6.0 Hz, 1H, phenyl-H). ^{13}C NMR (100 MHz, $CDCl_3$, ppm): δ 158.16, 148.23, 136.89, 135.80, 130.14, 129.49, 126.98, 123.43, 119.18, 53.65, 20.74, 15.96. Mass spectrometry (ESI-MS, m/z): $[M - I]^+$ calcd for $C_{12}H_{14}N^+$, 172.1126; found, 172.1122.

Synthesis of compound QMI

Compound 2 (100 mg, 0.33 mmol) and compound 1 (90 mg, 0.30 mmol) were dissolved in toluene (5 mL), along with the addition of piperidine (0.5 mL). Then the mixture was refluxed for 6 h under an argon atmosphere. Toluene was removed by evaporation, and then the crude product was purified by silica gel chromatography using dichloromethane/methyl alcohol (v/v, 9:1) as the eluent to afford **compound QMI** as a red solid (89 mg): Yield 51%. ^{1}H NMR (400 MHz, DMSO-d_6, ppm): δ 1.58 (t, J = 7.2 Hz, 3H, $NCH_2\boldsymbol{CH_3}$), 1.72-1.95 (m, 12H, adamantane-H), 2.12 (s, 1H, adamantane-H), 3.24 (s, 3H, -O-CH_3), 3.30 (s, 1H, adamantane-H), 4.98 (q, J = 7.2 Hz, 2H, $N\boldsymbol{CH_2}CH_3$), 6.73 (d, J = 2.4 Hz, 1H, phenyl-H), 6.94 (dd, J_1 = 2.4 Hz, J_2 = 8.4 Hz, 1H, phenyl-H), 7.97 (d, J = 16 Hz, 1H, alkene-H), 8.02 (t, J = 8 Hz, 1H, phenyl-H), 8.08 (d, J = 6.8 Hz, 1H, phenyl-H), 8.16 (d, J = 16 Hz, 1H, alkene-H), 8.21-8.27 (m, 2H, phenyl-H), 8.54 (d, J = 8.8 Hz, 1H, phenyl-H), 8.98 (d, J = 8 Hz, 1H, phenyl-H), 9.30 (d, J = 6.8 Hz, 1H, phenyl-H), 10.34 (s, 1H, -OH). ^{13}C NMR (100 MHz, DMSO-d_6, ppm): δ 159.70, 153.00, 147.29, 140.49, 137.99, 137.65, 135.10, 130.67, 129.64, 129.06, 126.69, 126.55, 125.62, 119.09, 117.48, 117.30, 116.16, 115.38, 56.46, 52.09, 38.49, 38.44, 36.38, 32.19, 29.14, 27.57, 15.01. Mass spectrometry (ESI-MS, m/z): $[M - I]^+$ calcd for $C_{31}H_{34}NO_2^+$, 452.2590; found, 452.2584.

Synthesis of compound 3

4-methylpyridine (1.00 g, 10.75 mmol) and iodoethane (2.58 mL, 32.25 mmol) were dissolved in acetonitrile (10 mL). Then the mixture was refluxed for 8 h under an argon atmosphere. After cooling to room temperature, the resultant precipitant was collected by filtration and washed with acetonitrile. The solid product was dried in vacuum to afford **compound 3** as a yellow solid (2.46 g): Yield 92%. ^{1}H NMR (400 MHz, $CDCl_3$, ppm): δ 1.72 (t, J = 7.6 Hz, 3H, $NCH_2\boldsymbol{CH_3}$), 2.69 (s, 3H, pyridine-$\boldsymbol{CH_3}$), 4.96 (q, J = 7.2 Hz, 2H, $N\boldsymbol{CH_2}CH_3$), 7.91 (d, J = 6.4 Hz, 2H, pyridine-H), 9.29 (d, J = 6.8 Hz, 2H, pyridine-H). ^{13}C NMR (100 MHz, $CDCl_3$, ppm): δ 159.05, 143.84, 129.05, 56.64, 22.46, 17.26. Mass spectrometry (ESI-MS, m/z): $[M - I]^+$ calcd for $C_8H_{12}N^+$, 122.0964; found, 122.0964.

Synthesis of compound PyCL

Compound 3 (100 mg, 0.40 mmol) and compound 1 (108 mg, 0.36 mmol) were dissolved in toluene (5 mL) with piperidine (0.5 mL). Then the mixture was refluxed for 8 h under an argon atmosphere. Toluene was removed by evaporation, and the crude product was purified by silica gel chromatography using dichloromethane/methyl alcohol (v/v, 10:1) as the eluent to afford **compound PyCL** as a yellow solid (90 mg): Yield 47%. ^{1}H NMR (400 MHz, DMSO-d_6, ppm): δ 1.51 (t, J = 7.2 Hz, 3H, $NCH_2\boldsymbol{CH_3}$), 1.66-1.94 (m, 12H, adamantane-H), 2.05 (s, 1H, adamantane-H), 3.22 (s, 3H, -O-CH_3), 3.28 (s, 1H, adamantane-H), 4.51 (q, J = 7.2 Hz, 2H, $N\boldsymbol{CH_2}CH_3$), 6.71 (d, J = 2.8 Hz, 1H, phenyl-H), 6.91 (dd, J_1 = 2.4 Hz, J_2 = 8.4 Hz, 1H, phenyl-H), 7.33 (d, J = 16.4 Hz, 1H, alkene-H), 7.79 (d, J = 16.4 Hz, 1H, alkene-H), 7.84 (d, J = 8.8 Hz, 1H, phenyl-H), 8.01 (d, J = 7.2 Hz, 2H, pyridine-H), 8.88 (d, J = 6.8 Hz, 2H, pyridine-H). ^{13}C NMR (100 MHz, DMSO-d_6, ppm): δ 159.59, 152.96, 144.03, 140.31, 138.27, 137.55, 130.35, 128.33, 125.12, 122.96, 120.51, 117.38, 116.28, 56.30, 54.99, 38.45, 36.41, 32.14, 29.13, 27.59, 16.09. Mass spectrometry (ESI-MS, m/z): $[M - I]^+$ calcd for $C_{27}H_{32}NO_2^+$, 402.2428; found, 402.2426.

Synthesis of compound 4

2,3,3-trimethyl-3H-indole (1.00 g, 6.28 mmol) and iodoethane (1.51 mL, 18.86 mmol) were dissolved in acetonitrile (10 mL). Then the mixture was refluxed for 10 h under an argon atmosphere. After cooling to room temperature, the resultant precipitant was collected by

filtration and washed with acetonitrile. The solid product was dried in vacuum to afford **compound 4** as a pale pink solid (1.72 g): Yield 87%. ^{1}H NMR (400 MHz, $CDCl_3$, ppm): δ 1.63 (t, J = 7.6 Hz, 3H, $NCH_2\boldsymbol{CH_3}$), 1.67 (s, 6H, Indole-$\boldsymbol{(CH_3)_2}$), 3.17 (s, 3H, Indole-$\boldsymbol{CH_3}$), 4.79 (q, J = 7.2 Hz, 2H, $N\boldsymbol{CH_2}CH_3$), 7.58-7.61 (m, 3H, phenyl-H), 7.70-7.72 (m, 1H, phenyl-H). ^{13}C NMR (100 MHz, $CDCl_3$, ppm): δ 195.40, 141.68, 140.55, 130.18, 129.59, 123.47, 115.38, 54.68, 45.44, 23.12, 17.01, 13.67. Mass spectrometry (ESI-MS, m/z): $[M - I]^+$ calcd for $C_{13}H_{18}N^+$, 188.1434; found, 188.1430.

Synthesis of compound InCL

Compound 4 (100 mg, 0.32 mmol) and compound 1 (86 mg, 0.29 mmol) were dissolved in toluene (5 mL) with piperidine (0.5 mL). Then the mixture was refluxed for 8 h under an argon atmosphere. Toluene was removed by evaporation, and the crude product was purified by silica gel chromatography using dichloromethane/methyl alcohol (v/v, 10:1) as the eluent to afford **compound InCL** as a red solid (112 mg): Yield 65%. ^{1}H NMR (400 MHz, $CDCl_3$, ppm): δ 1.46 (t, J = 7.2 Hz, 3H, $NCH_2\boldsymbol{CH_3}$), 1.68 (d, J = 12.8 Hz, 6H, Indole-$\boldsymbol{(CH_3)_2}$), 1.74-2.00 (m, 12H, adamantane-H), 2.48 (s, 1H, adamantane-H), 3.32 (s, 4H, -O-$\boldsymbol{CH_3}$, adamantane-$\boldsymbol{H}$), 4.17 (q, J = 7.2 Hz, 2H, $N\boldsymbol{CH_2}CH_3$), 6.54-6.59 (m, 2H, phenyl-H, alkene-H), 6.79 (d, J = 8.8 Hz, 1H, phenyl-H), 7.10 (d, J = 8 Hz, 1H, phenyl-H), 7.24 (t, J = 7.6 Hz, 1H, phenyl-H), 7.35-7.41 (m, 2H, phenyl-H), 7.95 (d, J = 9.2 Hz, 1H, phenyl-H), 8.25 (d, J = 14.4 Hz, 1H, alkene-H). ^{13}C NMR (100 MHz, $CDCl_3$, ppm): δ 171.90, 148.40, 144.53, 141.89, 141.20, 140.85, 133.14, 132.34, 128.58, 125.66, 124.59, 124.05, 122.24, 120.81, 109.80, 97.28, 57.04, 48.95, 39.74, 39.34, 39.13, 37.13, 32.65, 31.59, 29.63, 28.42, 28.38, 28.28, 27.80, 22.66, 14.13, 12.34. Mass spectrometry (ESI-MS, m/z): $[M - I]^+$ calcd for $C_{32}H_{38}NO_2^+$, 468.2897; found, 468.2891.

3. Supplementary Figures

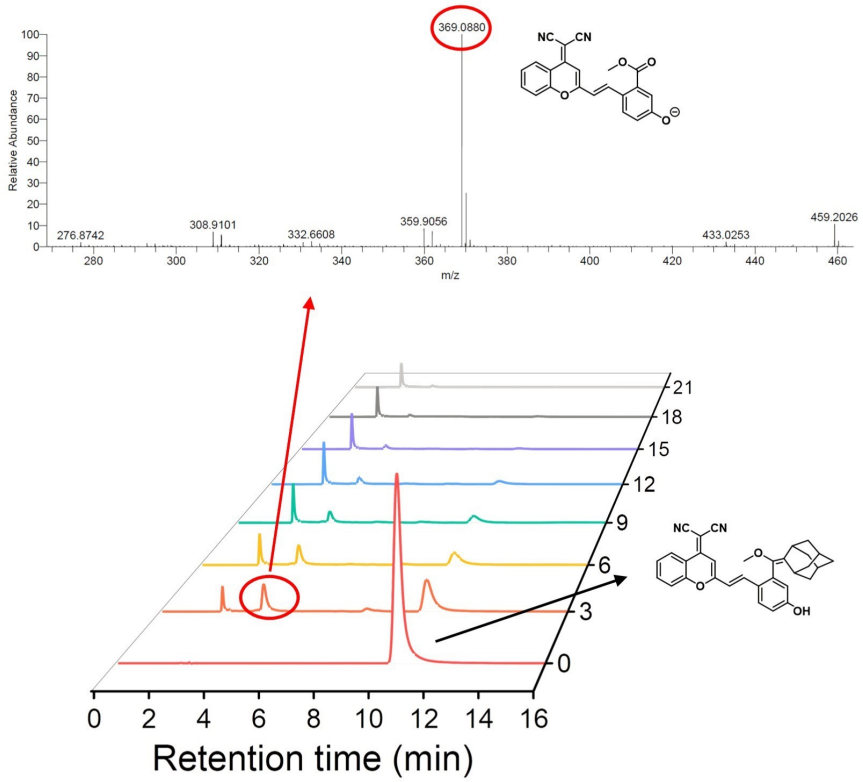

Figure S1. HPLC profiles of DCMCL (1 mM) upon successive irradiation (white light, 1.6 W cm^{-2}) in a mixture of PBS/DMSO (v/v = 1/1). Samples were taken at 3 min intervals during the light period for HPLC analysis. The peak labeled in the profiles was confirmed by HRMS to be the theoretical decomposition product from the chemiexcitation process.

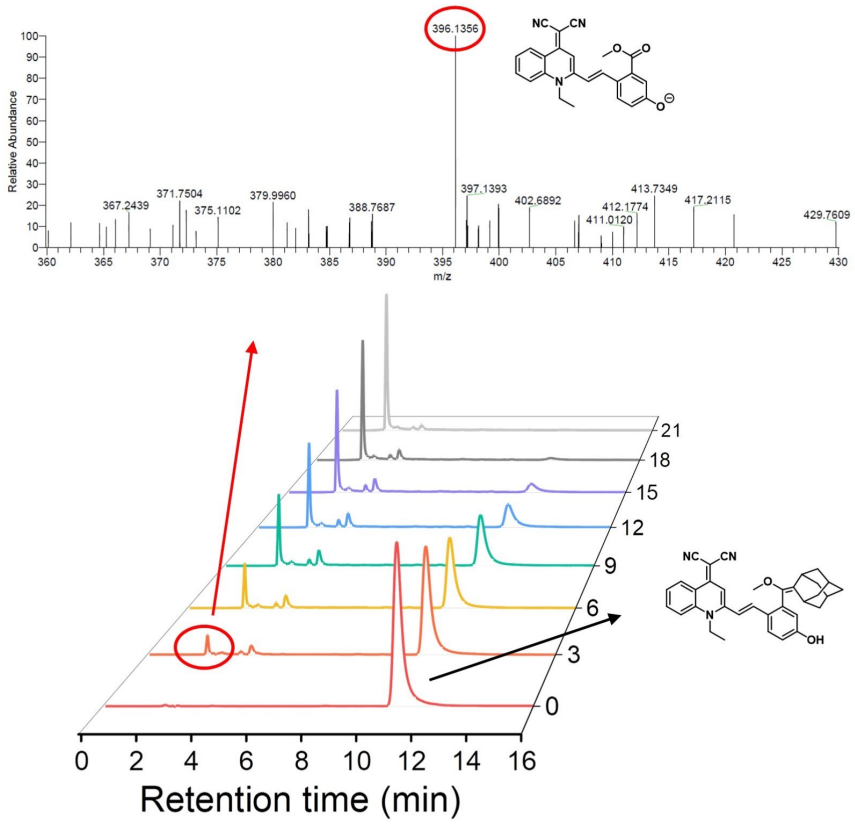

Figure S2. HPLC profiles of QMCL (1 mM) upon successive irradiation (white light, 1.6 W cm^{-2}) in a mixture of PBS/DMSO (v/v = 1/1). Samples were taken at 3 min intervals during the light period for HPLC analysis. The peak labeled in the profiles was confirmed by HRMS to be the theoretical decomposition product from the chemiexcitation process.

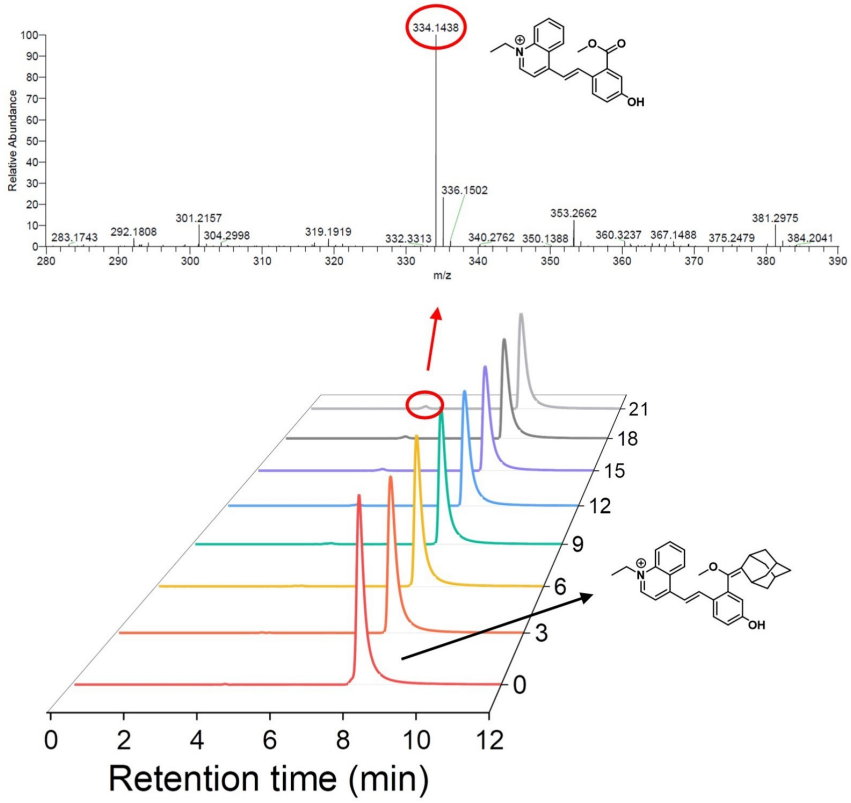

Figure S3. HPLC profiles of QMI (1 mM) upon successive irradiation (white light, 1.6 W cm^{-2}) in a mixture of PBS/DMSO (v/v = 1/1). Samples were taken at 3 min intervals during the light period for HPLC analysis. The peak labeled in the profiles was confirmed by HRMS to be the theoretical decomposition product from the chemiexcitation process.

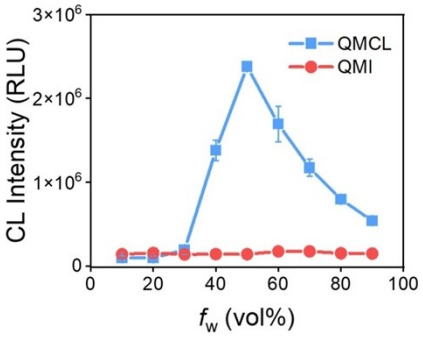

Figure S4. Chemiluminescence intensity of QMCL and QMI in a mixture of PBS/DMSO with different PBS fractions (f_w) under irradiation without photosensitizers. The concentration of probes was 50 μM, and white light irradiation for 2 min. Data with error bars are expressed as mean ± s.d., n = 3.

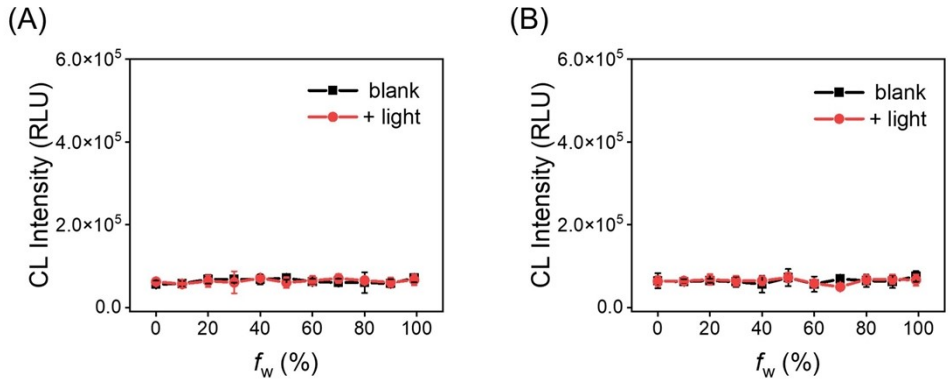

Figure S5. Chemiluminescence intensity of PyCL (A) and InCL (B) in a mixture of PBS/DMSO with different PBS fractions (f_w) in the absence or presence of light irradiation (no photosensitizers). The concentration of probes was 50 μM, and white light irradiation for 2 min. Data with error bars are expressed as mean ± s.d., n = 3.

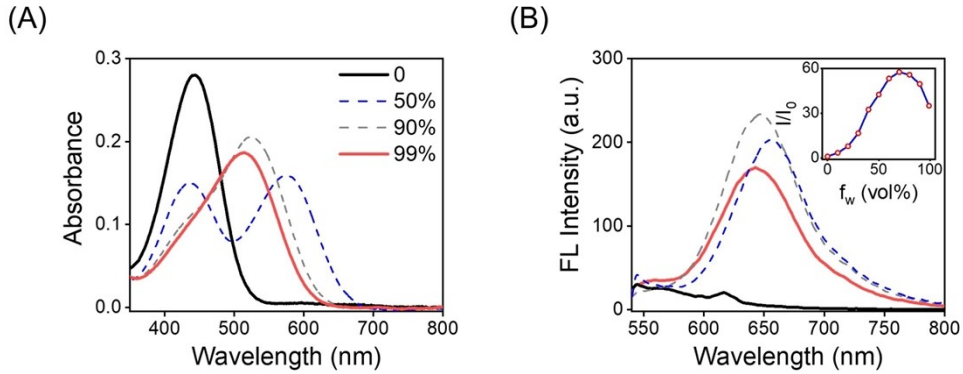

Figure S6. Absorbance spectra (A) and Emission spectra (B) of QMI (10 μM) in a mixture of PBS/DMSO with different PBS fractions.

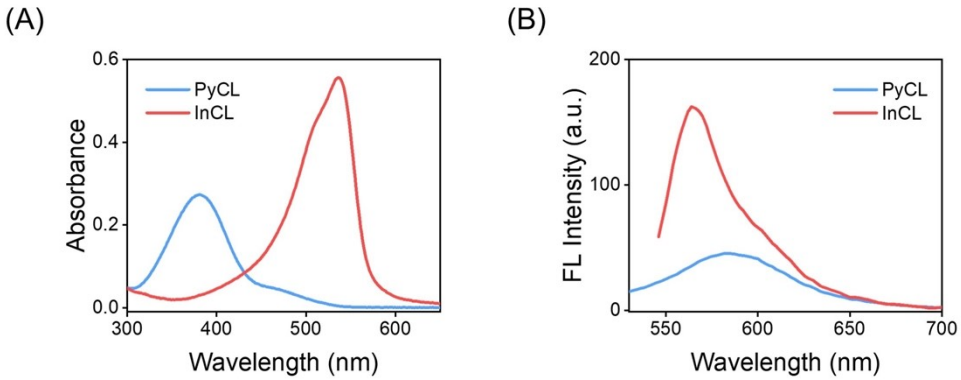

Figure S7. Absorbance spectra (A) and Emission spectra (B) of PyCL (10 μM) and InCL (10 μM) in a mixture of PBS/DMSO (v/v = 9/1).

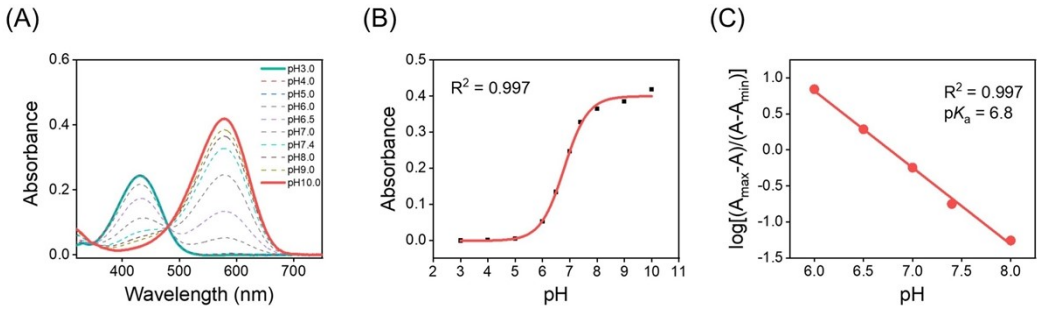

Figure S8. (A) pH-dependent UV-vis absorption spectra of QMI (10 μM) at various pH values. (B) The absorbance at 580 nm of QMI as a function of pH values. (C) Linear fitted curve of log[(A_{max}-A)/(A-A_{min})] versus pH for QMI.

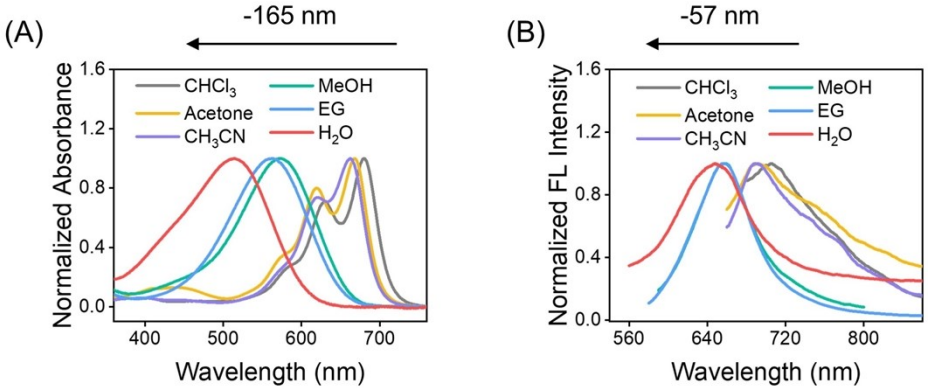

Figure S9. The normalized absorption (A) and emission spectra (B) of QMI in various solvents: $CHCl_3$, Acetone, CH_3CN, MeOH, ethylene glycol (EG), H_2O.

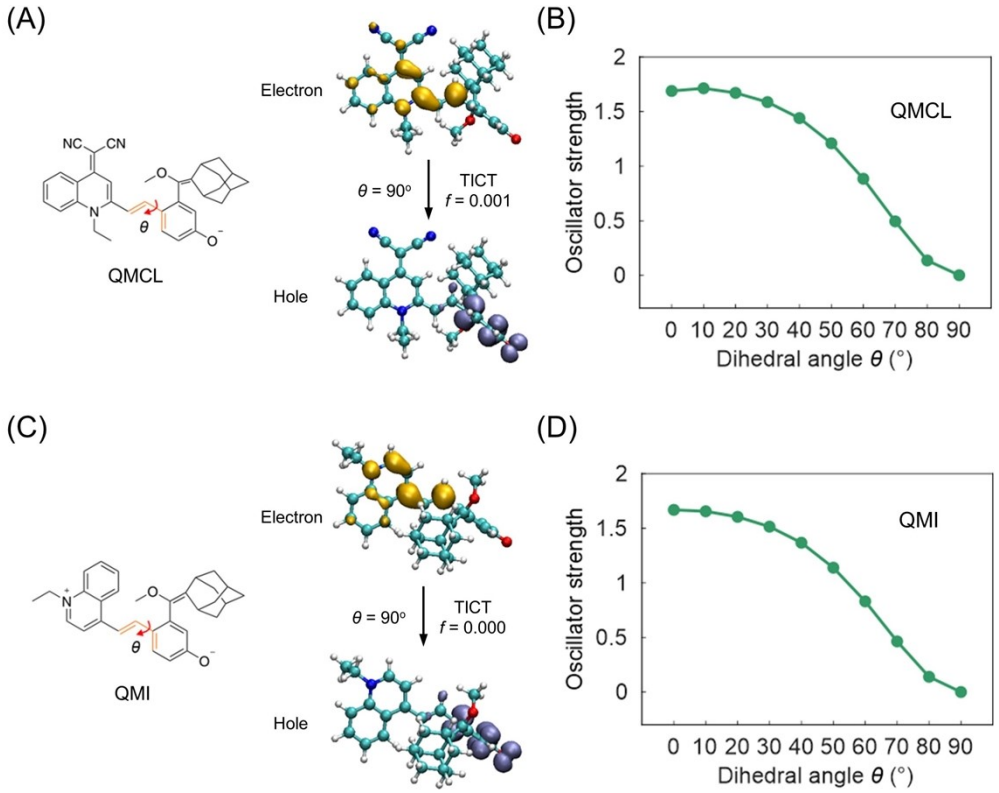

Figure S10. The electron and hole distribution of QMCL (A) and QMI (C) in the TICT state in water. The corresponding oscillator strength of QMCL (B) and QMI (D) as a function of rotating angle (θ) in water. The dihedral angle (θ) is highlighted in orange in A (QMCL) and C (QMI).

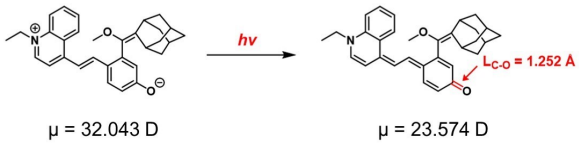

Figure S11. Representative resonance structures of deprotonated QMI.

Table S1. The dipole moments of the zwitterionic probe QMI in different solvents

QMI	In the ground state	In the excited state
Toluene	17.505 D	18.761 D
Water	32.043 D	23.574 D

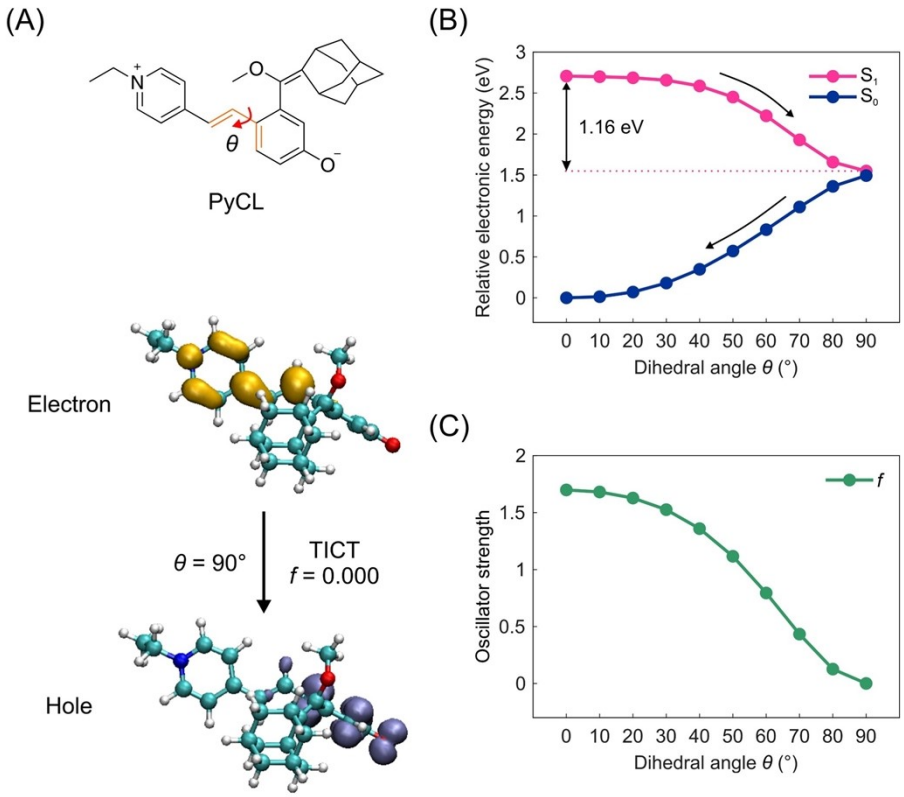

Figure S12. (A) The electron and hole distribution of PyCL in the TICT state in water. (B) Calculated S_1 (pink) and S_0 (dark blue) potential energy surface and (C) the corresponding oscillator strength of PyCL as a function of rotating angle (θ) in water. The dihedral angle (θ) is highlighted in orange in (A).

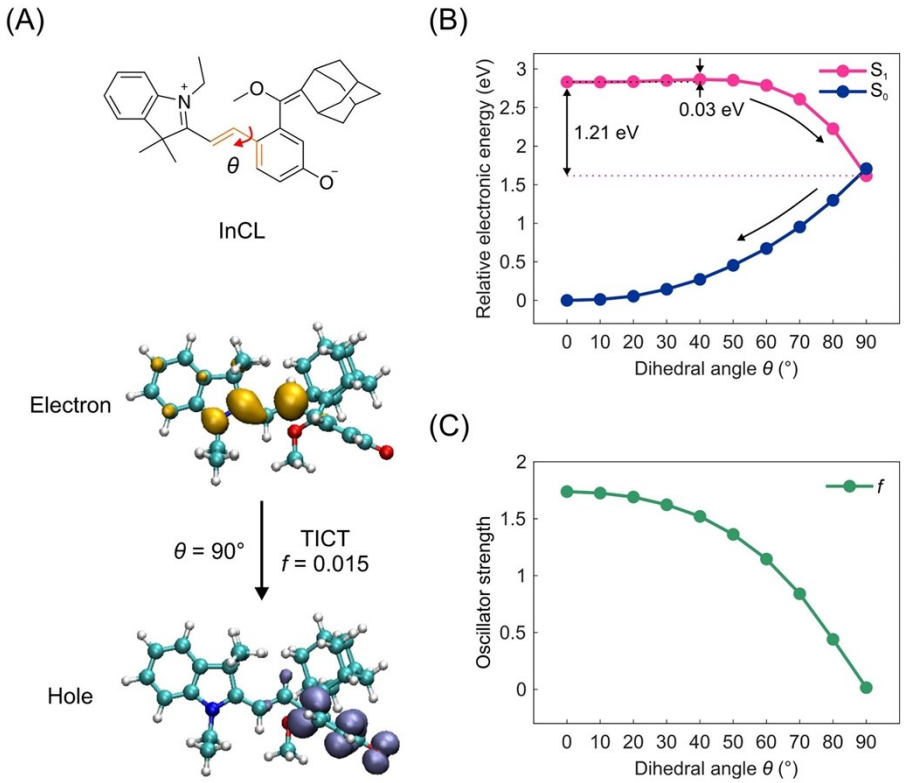

Figure S13. (A) The electron and hole distribution of InCL in the TICT state in water. (B) Calculated S_1 (pink) and S_0 (dark blue) potential energy surface and (C) the corresponding oscillator strength of InCL as a function of rotating angle (θ) in water. The dihedral angle (θ) is highlighted in orange in (A).

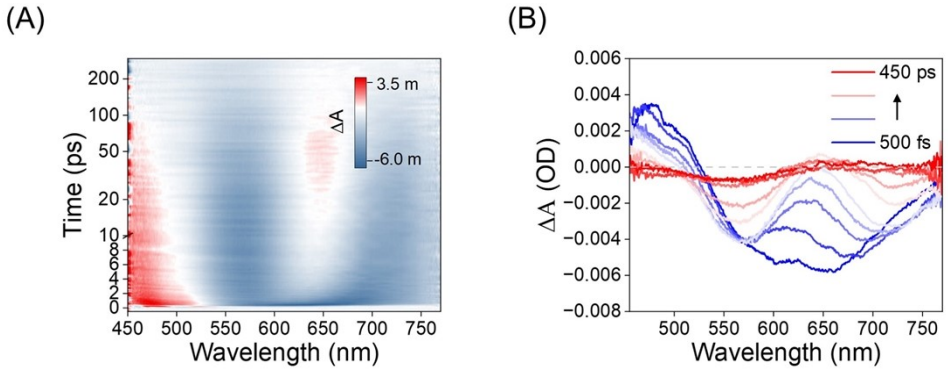

Figure S14. Femtosecond time-resolved transient absorption spectroscopy of DCMCL (100 μM) in a mixture of PBS/DMSO (v/v = 1/1). λ_{ex} = 450 nm.

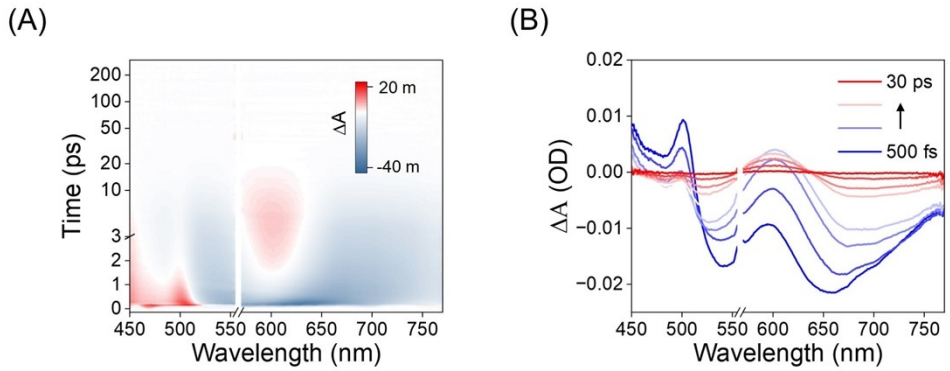

Figure S15. Femtosecond time-resolved transient absorption spectroscopy of QMI (100 μM) in PBS solution (pH 7.4). λ_{ex} = 560 nm.

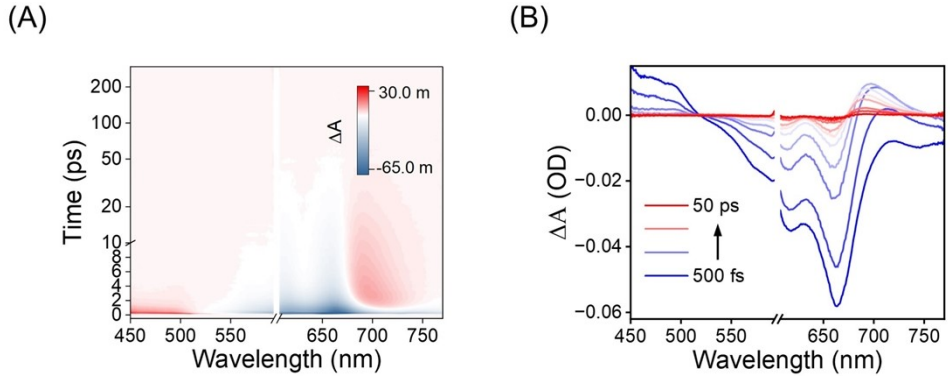

Figure S16. Femtosecond time-resolved transient absorption spectroscopy of QMI (100 μM) in CH_3CN. λ_{ex} = 600 nm.

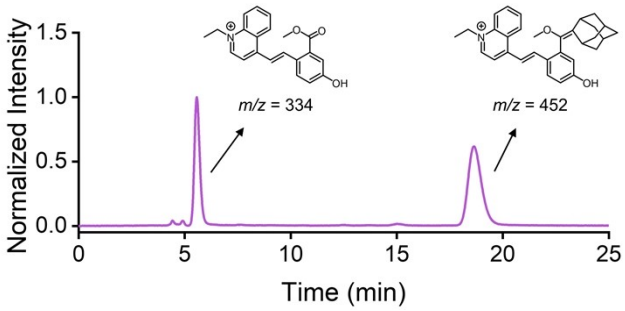

Figure S17. HPLC-ESI MS analysis of the reaction solution of QMI and singlet oxygen.

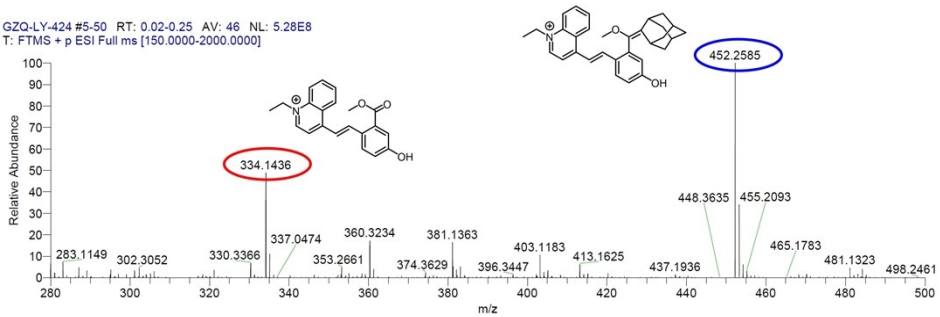

Figure S18. HRMS analysis of the reaction solution of QMI and singlet oxygen.

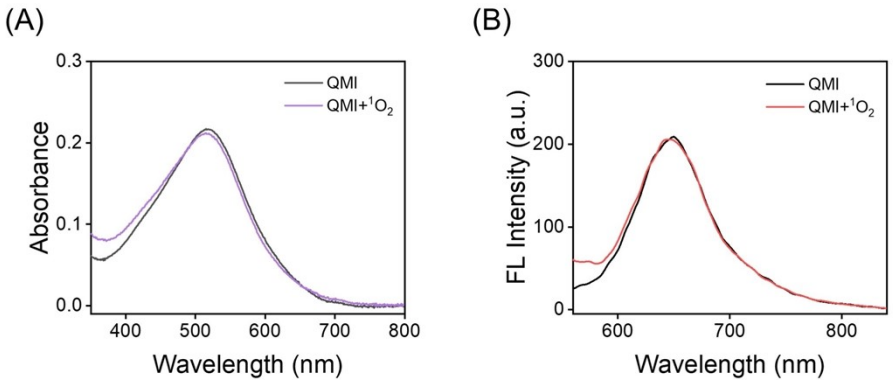

Figure S19. Absorption spectra (A) and Emission spectra (B) of QMI before and after reaction with singlet oxygen in PBS solution.

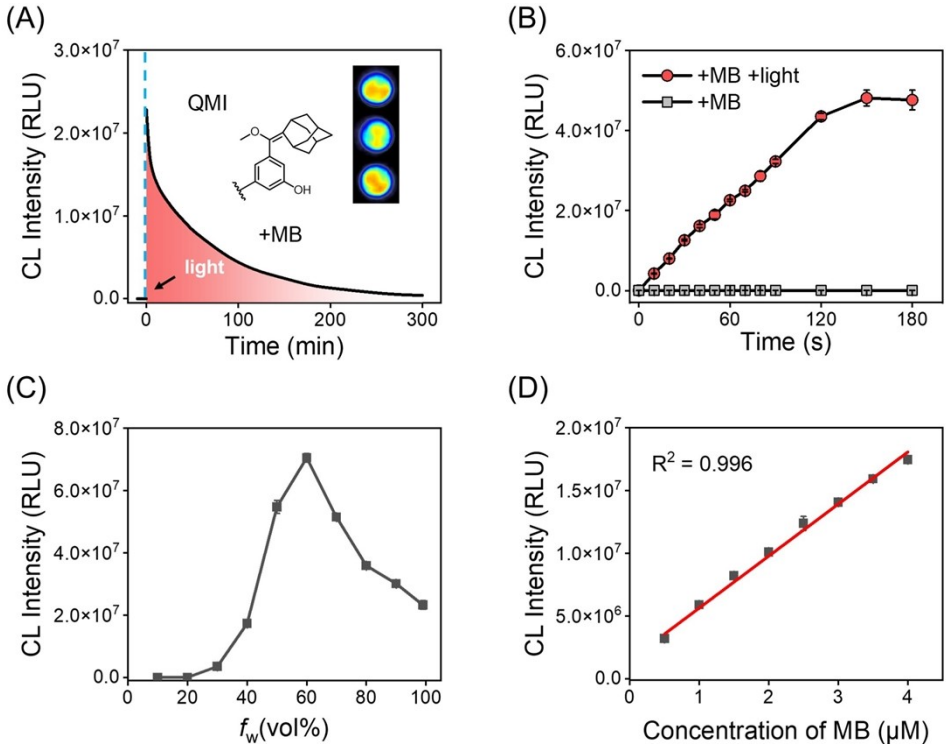

Figure S20. (A) Chemiluminescence kinetic studies of QMI (50 μM) after the addition of $^1O_2$ (MB 10 μM, 200 mW cm^{-2} 690 nm laser irradiation for 1 min) in PBS (pH 7.4, containing 1 mM TBHP). Inset: Chemiluminescence imaging of QMI in a black 96-well plate. (B) Irradiation time dependent chemiluminescence intensity of QMI (50 μM). (C) Chemiluminescence intensity of QMI in a mixture of PBS/DMSO with different PBS fractions (f_w) in the presence of $^1O_2$ produced by MB (10 μM). (D) The linear correlation between the chemiluminescence signal intensity of QMI and the concentration of MB (Irradiation 1 min). Data with error bars are expressed as mean ± s.d., n = 3.

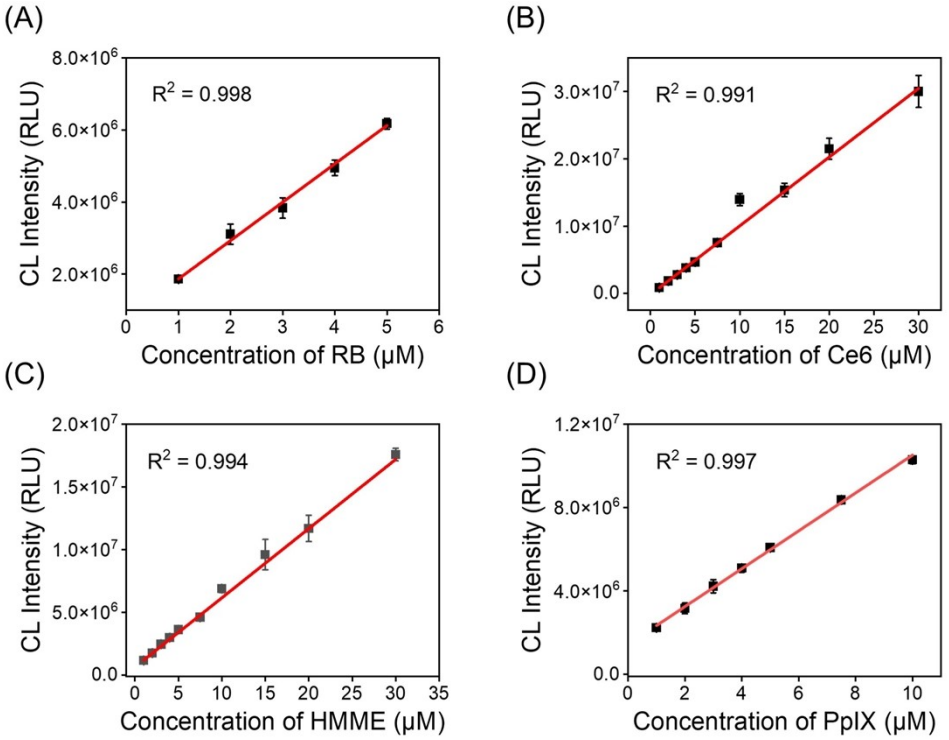

Figure S21. The linear correlation between the chemiluminescence signal intensity of QMI and the concentration of various photosensitizers. (A) RB (white light for 1 min), (B) Ce6 (white light for 2 min), (C) HMME (200 mW cm^{-2} 635 nm laser for 2 min) and (D) PpIX (200 mW cm^{-2} 635 nm laser for 2 min). Data with error bars are expressed as mean ± s.d., n = 3.

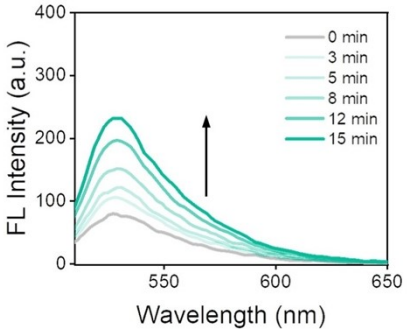

Figure S22. Self-sensitization of commercial $^1O_2$ probe SOSG in visible light. The fluorescence emission of SOSG increased continuously with irradiation time (10 μM, white light, 25 mW cm^{-2}) in absence of photosensitizers.

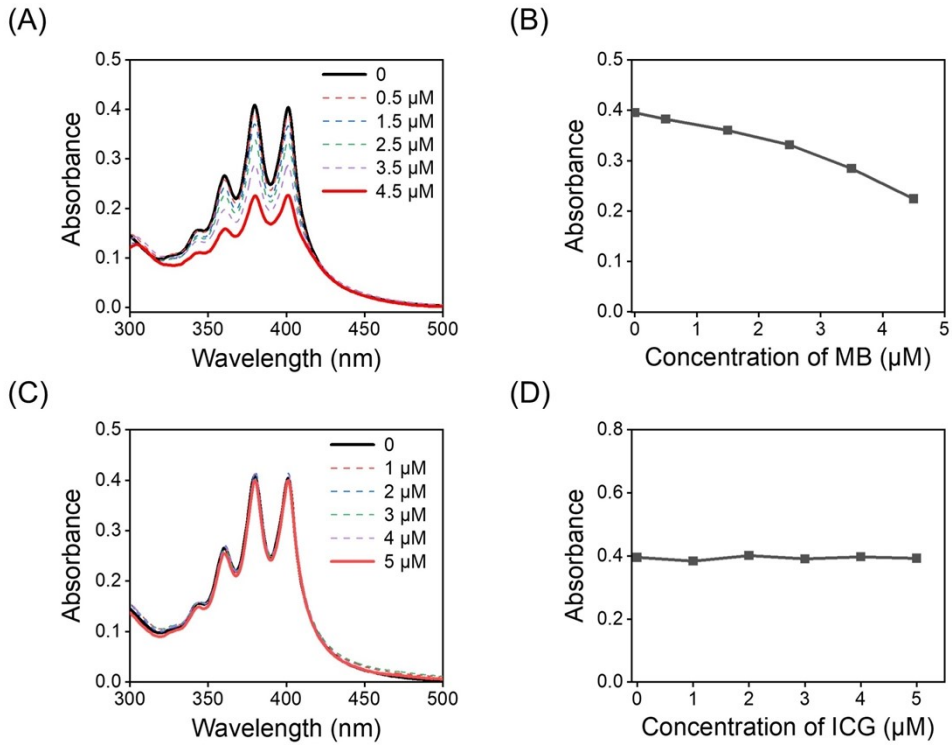

Figure S23. Variation of UV-vis absorption spectra of ABDA (a commercial $^1O_2$ probe, 50 μM) with concentrations of MB (10 μM, 200 mW cm^{-2} 690 nm laser for 1 min, A) or ICG (10 μM, 200 mW cm^{-2} 808 nm laser for 3 min, C). Correlation between the absorption variation at 400 nm of ABDA and concentrations of MB (B) or ICG (D).

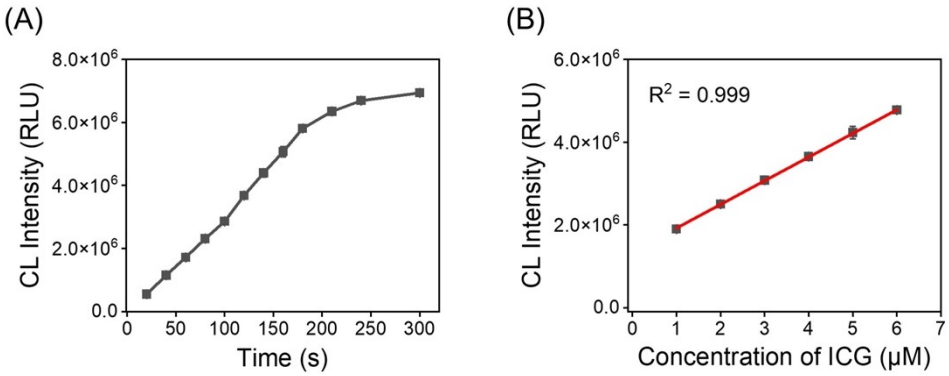

Figure S24. (A) Irradiation time dependent chemiluminescence intensity of QMI toward ICG (10 μM, 808 nm laser, 200 mW cm^{-2}). (B) The linear correlation between the chemiluminescence signal intensity of QMI and the concentration of ICG (Irradiation 3 min). Data with error bars are expressed as mean ± s.d., n = 3.

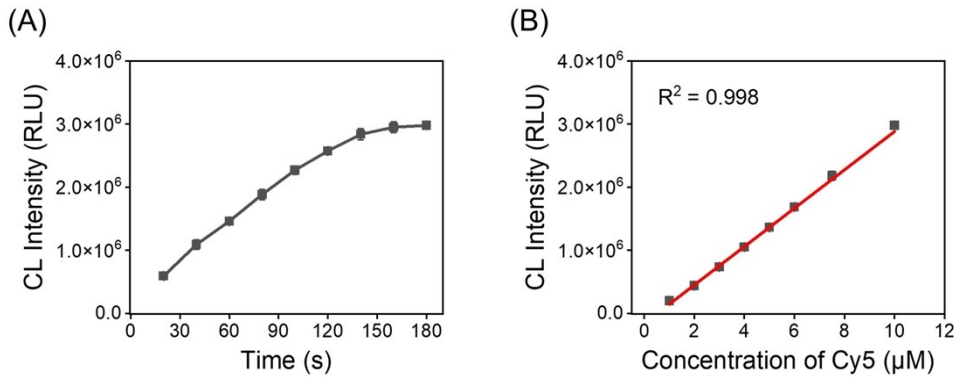

Figure S25. (A) Irradiation time dependent chemiluminescence intensity of QMI toward Cy5 (10 μM, 635 nm laser, 200 mW cm^{-2}). (B) The linear correlation between the chemiluminescence signal intensity of QMI and the concentration of Cy5 (Irradiation 3 min). Data with error bars are expressed as mean ± s.d., n = 3.

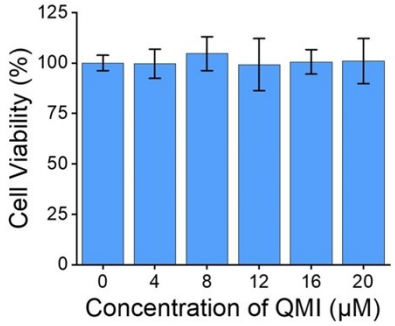

Figure S26. Cell viability of HeLa cells after incubation with QMI at various concentrations by MTT assay, at 37 °C for 24 h (each sample was tested using three replicates, and the results are reported as the mean ± standard deviation).

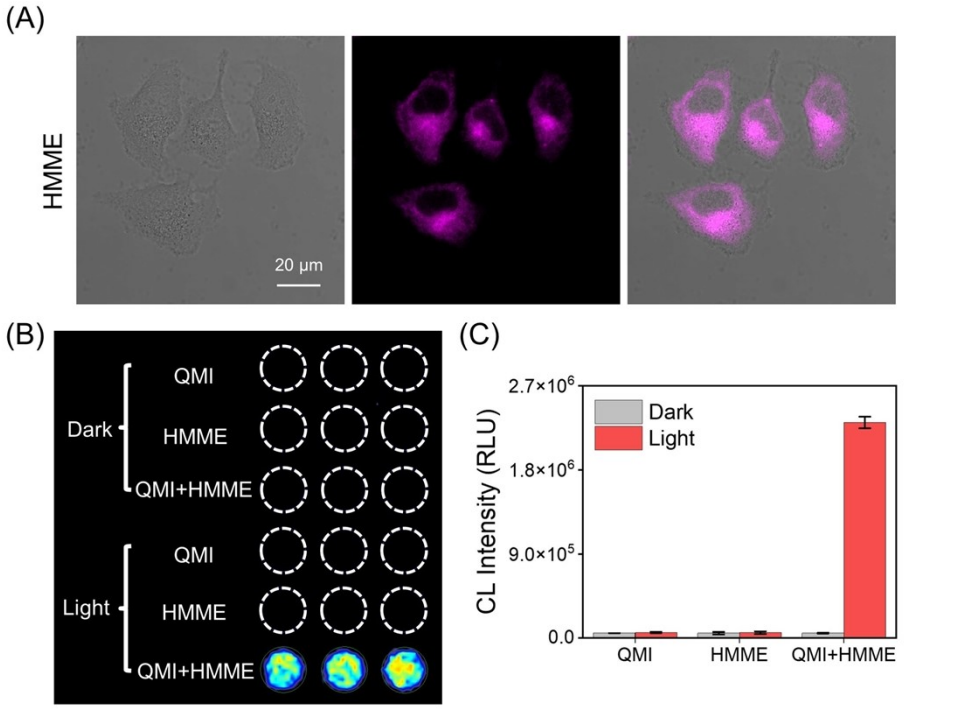

Figure S27. (A) HeLa cells were incubated with HMME (20 μM) for 2 h and then washed three times with PBS. λ_{ex} = 410 nm, λ_{em} = 620-710 nm. Scale bar: 20 μm. (B) HeLa cells were incubated with QMI (20 μM) for 1 h, HMME (20 μM) for 2 h, or HMME followed by QMI for 1 h. Subsequently, chemiluminescence imaging was obtained with or without light. (C) Quantification of chemiluminescence signal intensity emitted from the cells. Data with error bars are expressed as mean ± s.d., n = 3.

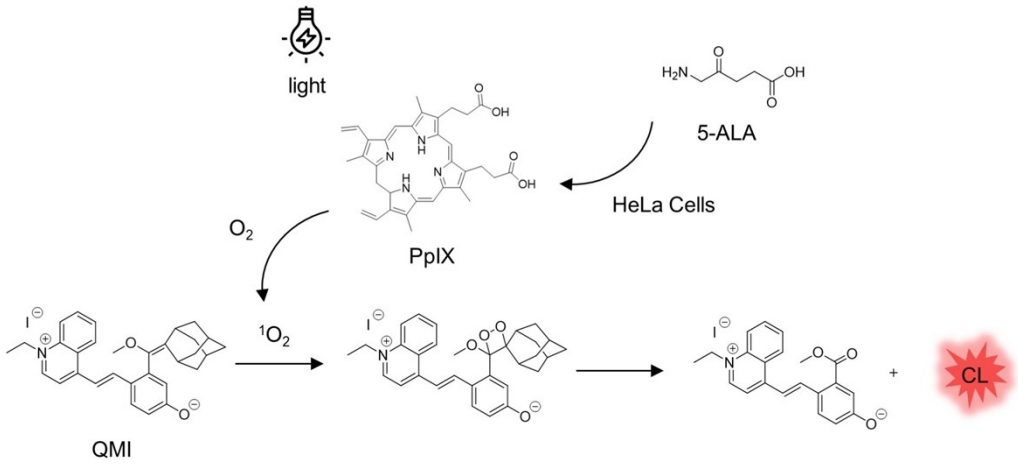

Scheme S2. Mechanistic process for detecting $^1O_2$ produced by the endogenous photosensitizer PpIX in living cells.

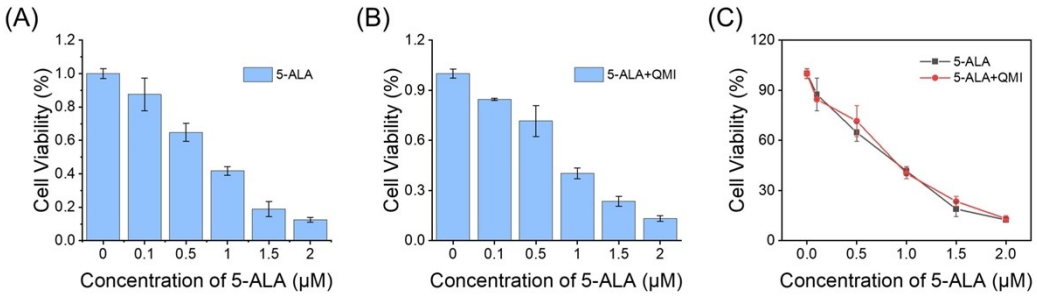

Figure S28. The effect of QMI on the PDT efficiency of 5-ALA. (A) Cell viability of HeLa cells treated with different concentrations of 5-ALA. (B) Cell viability of HeLa cells treated with different concentrations of 5-ALA and QMI (20 μM). (C) Cell viability of HeLa cells treated with 5-ALA or 5-ALA+QMI.

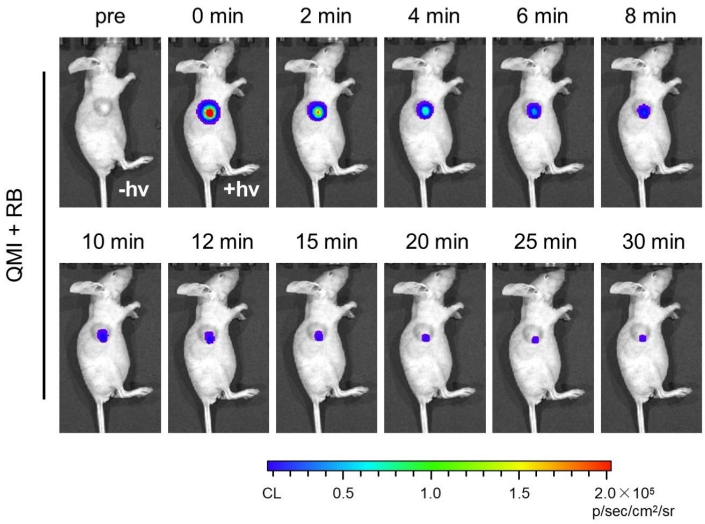

Figure S29. *In vivo* chemiluminescence imaging of HeLa tumor-bearing mice with in-situ injection of the mixed solution (QMI 100 μM+ RB 10 μM, 20 μL) after white light irradiation for 2 min.

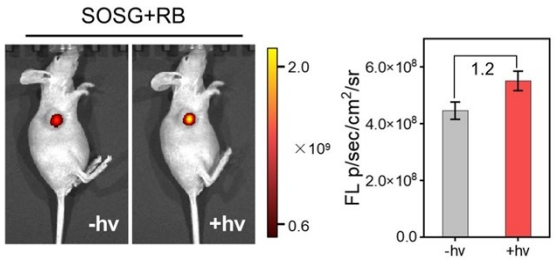

Figure S30. *In vivo* fluorescence imaging of HeLa tumor-bearing mice with in-situ injection of the mixed solution (SOSG 100 μM+ RB 10 μM, 20 μL) after white light irradiation for 2 min. Data with error bars are expressed as mean ± s.d., n = 3.

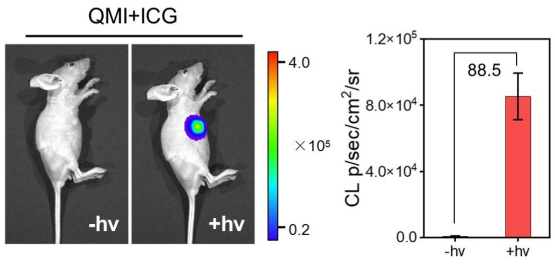

Figure S31. *In vivo* chemiluminescence imaging of HeLa tumor-bearing mice with in-situ injection of the mixed solution (QMI 100 μM+ ICG 40 μM, 20 μL) after 200 mW cm^{-2} 808 nm laser irradiation for 2 min. Data with error bars are expressed as mean ± s.d., n = 3.

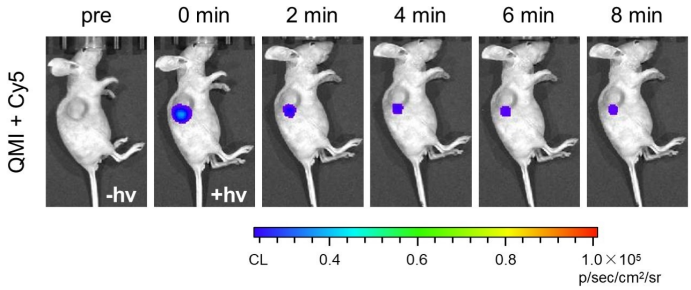

Figure S32. *In vivo* chemiluminescence imaging of HeLa tumor-bearing mice with in-situ injection of the mixed solution (QMI 100 μM + Cy5 40 μM, 20 μL) after 200 mW cm^{-2} 635 nm laser irradiation for 2 min.

4. ^{1}H NMR Spectra, ^{13}C NMR Spectra, and HRMS Spectra

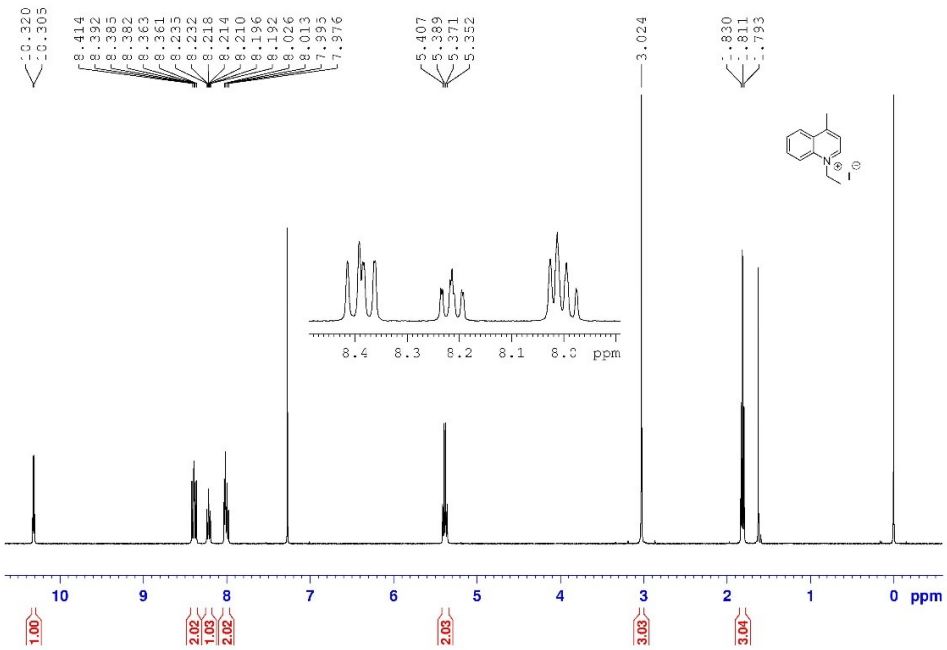

Figure S33. ^{1}H NMR spectrum of **Compound 2** in $CDCl_3$

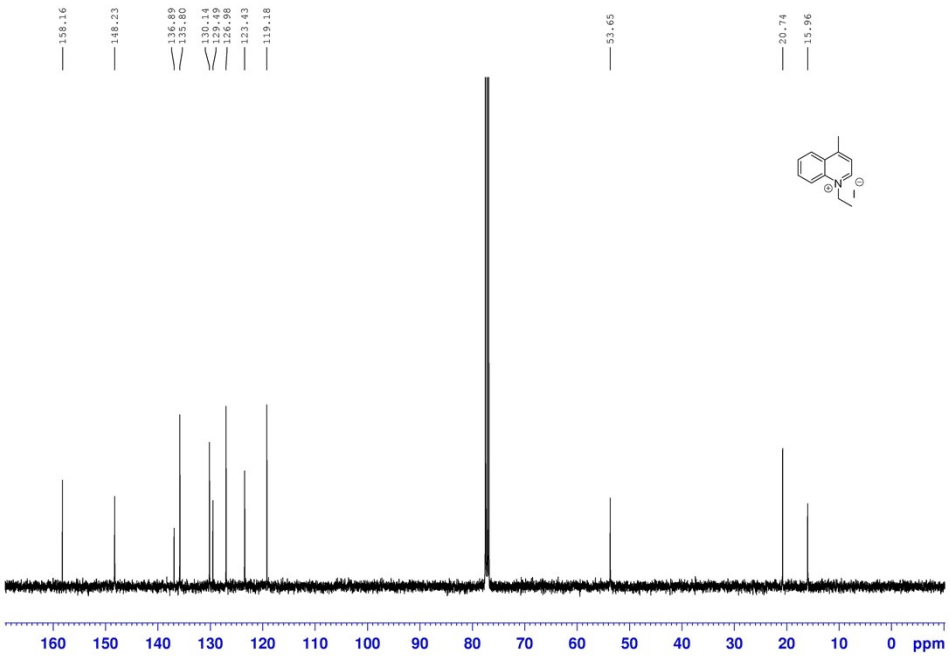

Figure S34. ^{13}C NMR spectrum of **Compound 2** in $CDCl_3$

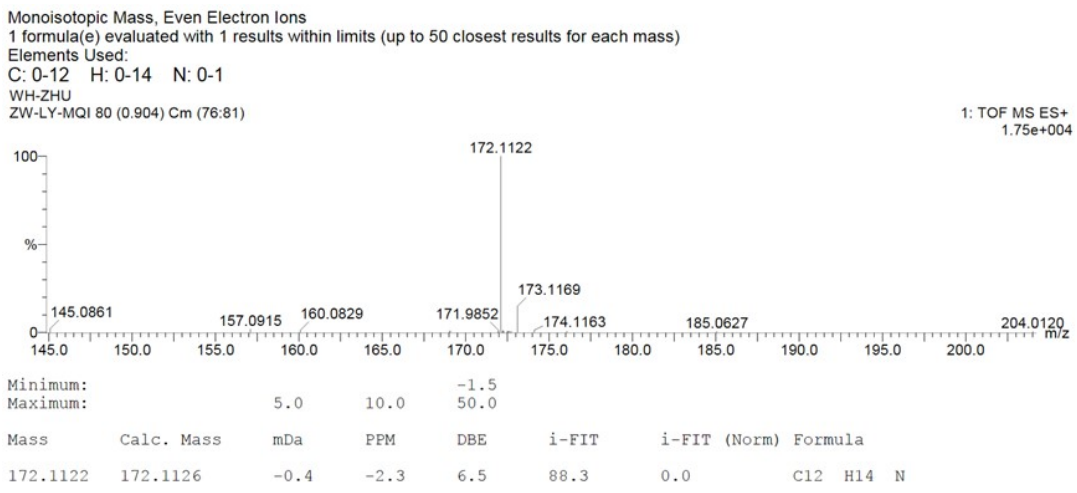

Figure S35. HRMS spectrum of **Compound 2**

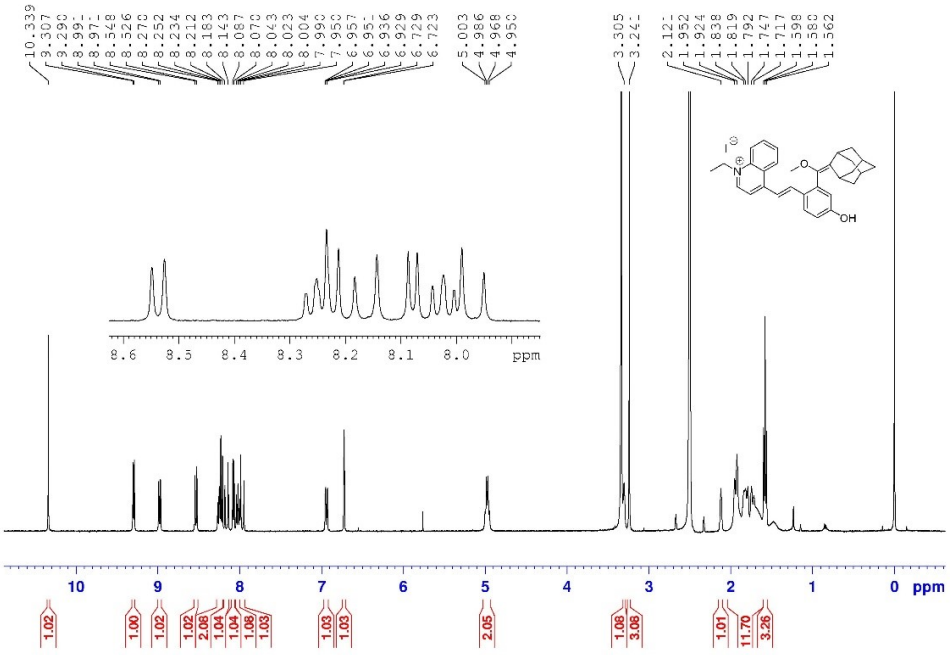

Figure S36. ^{1}H NMR spectrum of **QMI** in DMSO-d_6

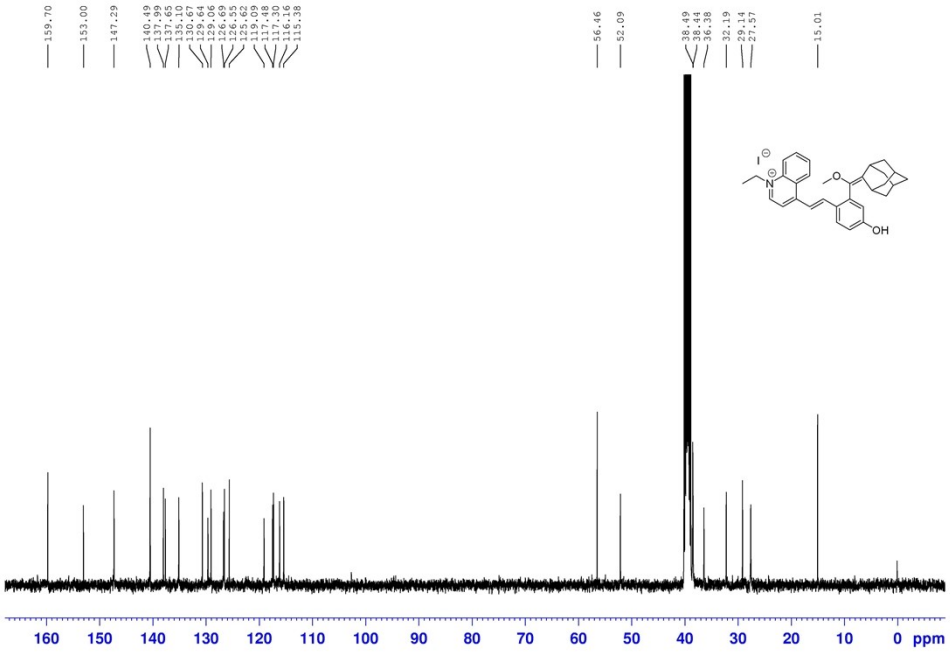

Figure S37. ^{13}C NMR spectrum of **QMI** in DMSO-d_6

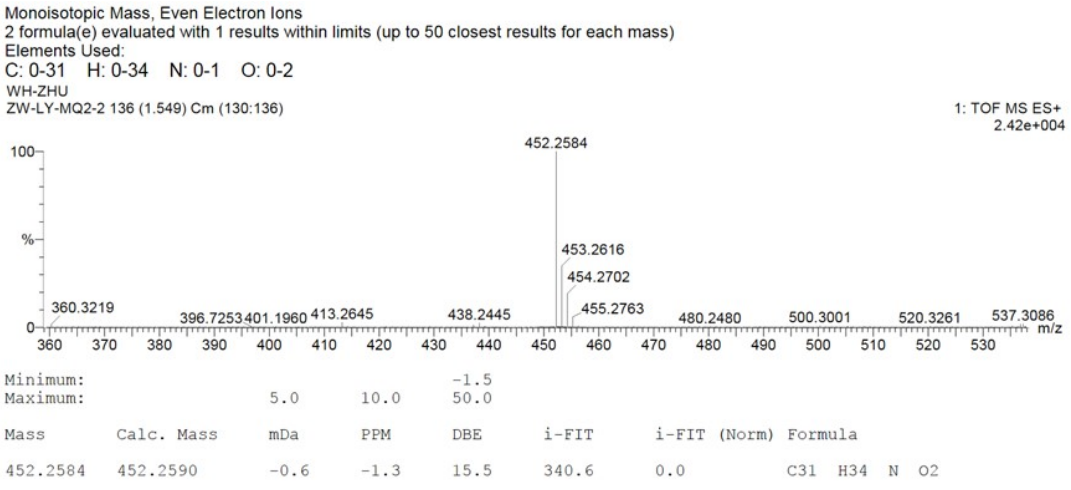

Minimum:				-1.5			
Maximum:		5.0	10.0	50.0			
Mass	Calc. Mass	mDa	PPM	DBE	i-FIT	i-FIT (Norm)	Formula
452.2584	452.2590	-0.6	-1.3	15.5	340.6	0.0	C31 H34 N O2

Figure S38. HRMS spectrum of **QMI**

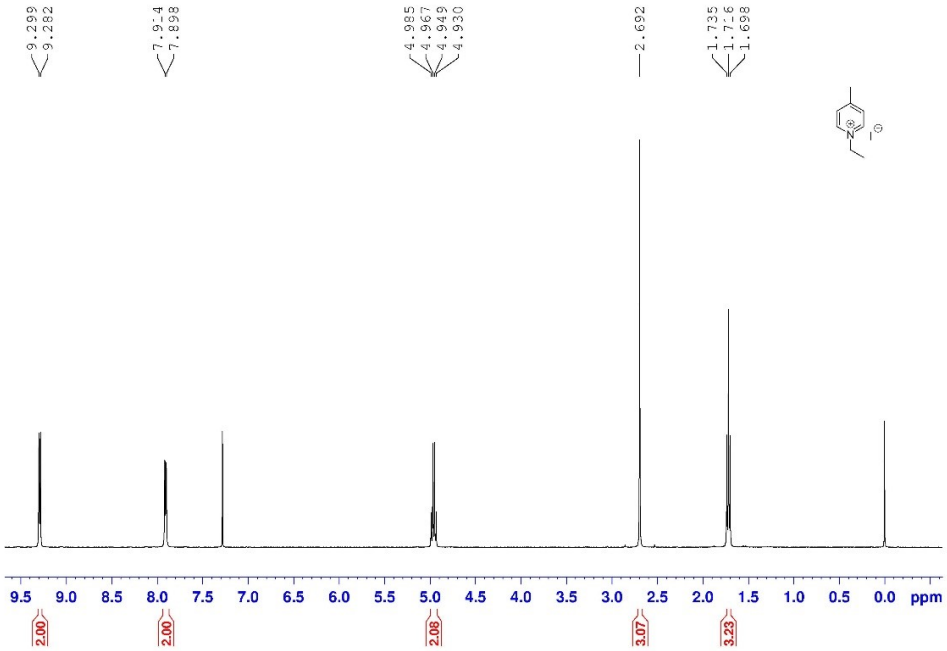

Figure S39. ^{1}H NMR spectrum of **Compound 3** in $CDCl_3$

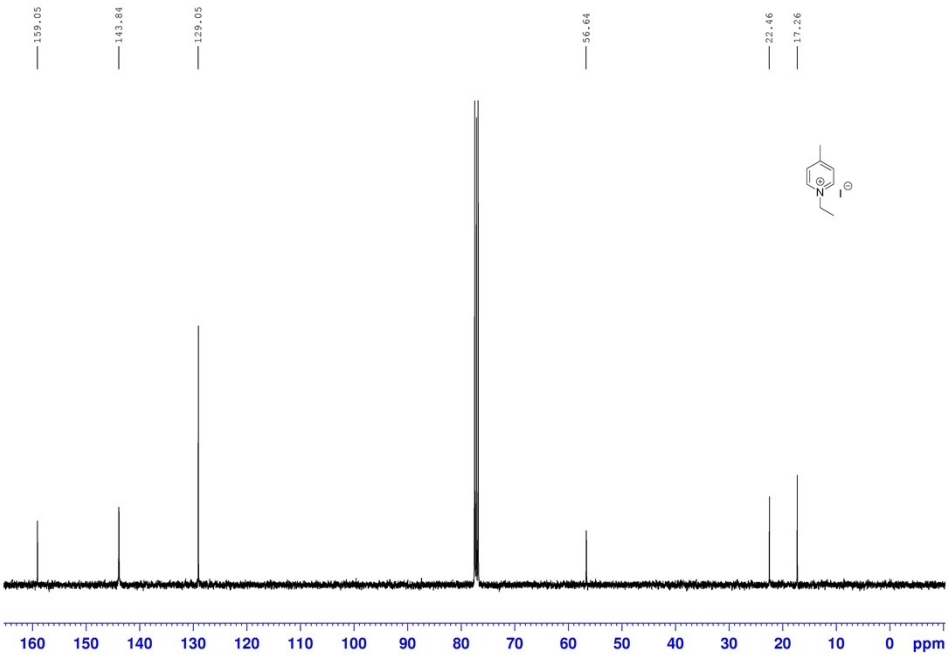

Figure S40. ^{13}C NMR spectrum of **Compound 3** in $CDCl_3$

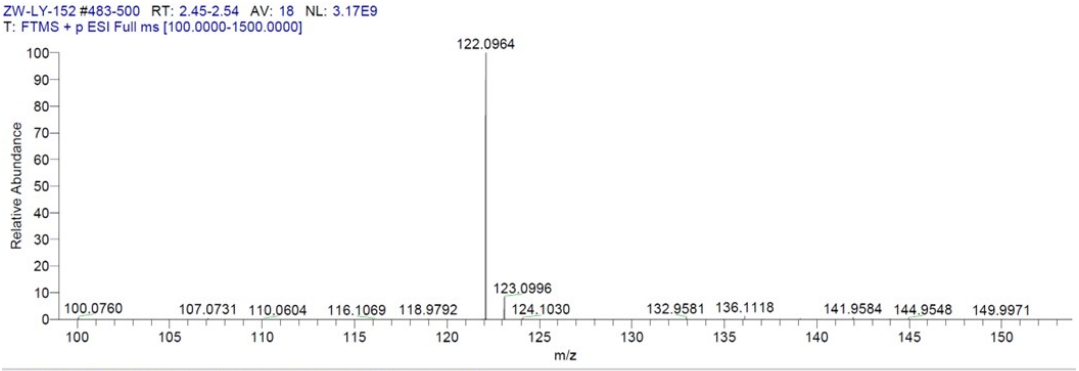

ZW-LY-152#483-498 RT: 2.45-2.53 AV: 16
T: FTMS + p ESI Full ms [100.0000-1500.0000]
m/z= 102.67-132.86

m/z	Intensity	Relative	Theo. Mass	Delta (ppm)	Composition
122.0964	3156952320.0	100.00	122.0964	-0.05	$C_8H_{12}N$

Figure S41. HRMS spectrum of **Compound 3**

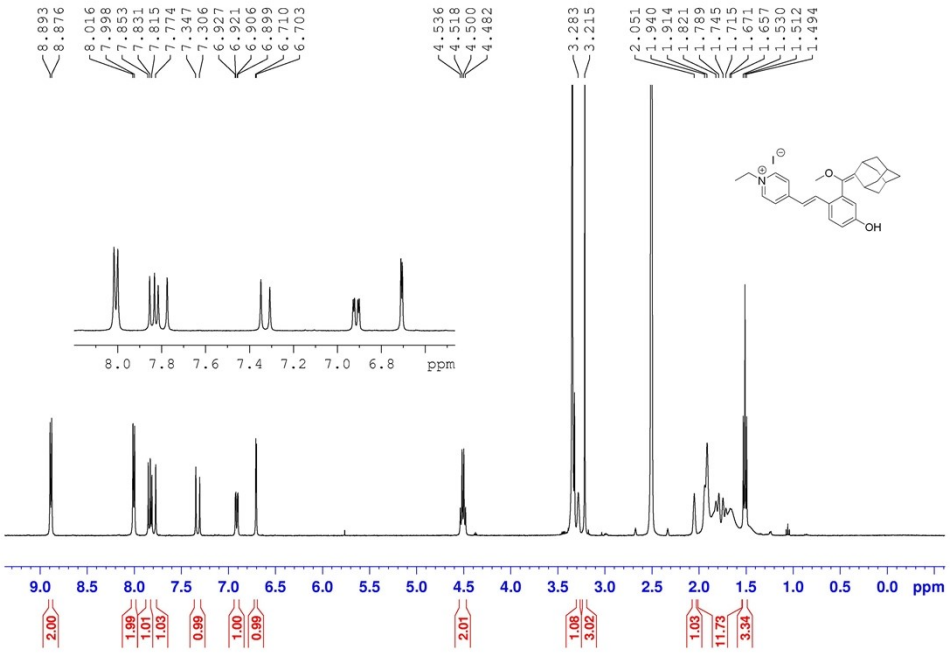

Figure S42. ^{1}H NMR spectrum of **PyCL** in DMSO-d_6

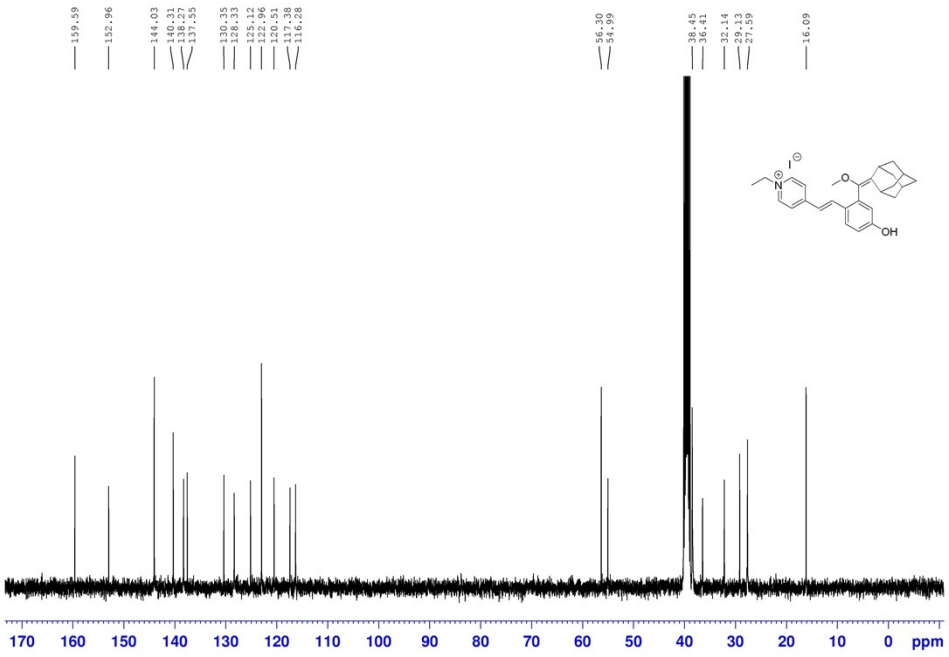

Figure S43. ^{13}C NMR spectrum of **PyCL** in DMSO-d_6

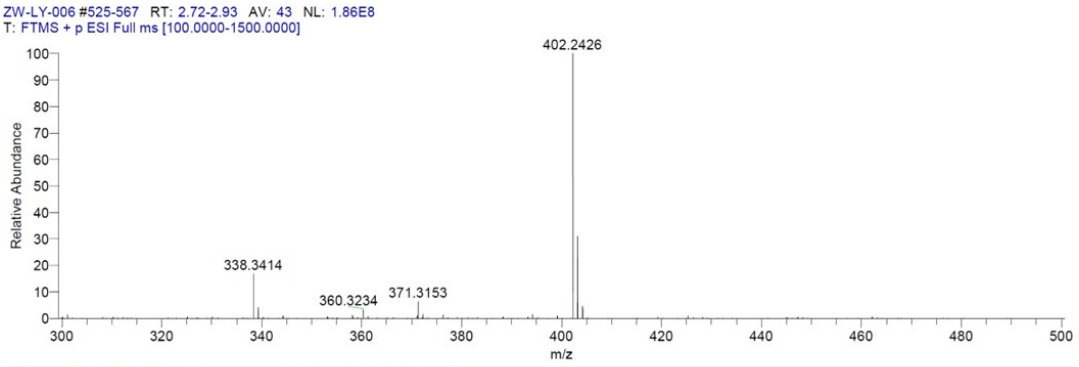

ZW-LY-006#525-582 RT: 2.72-3.01 AV: 58
T: FTMS + p ESI Full ms [100.0000-1500.0000]
m/z= 329.91-470.07

m/z	Intensity	Relative	Theo. Mass	Delta (ppm)	Composition
402.2426	157357952.0	100.00	402.2428	-0.20	$C_{27}H_{32}O_2N$

Figure S44. HRMS spectrum of **PyCL**

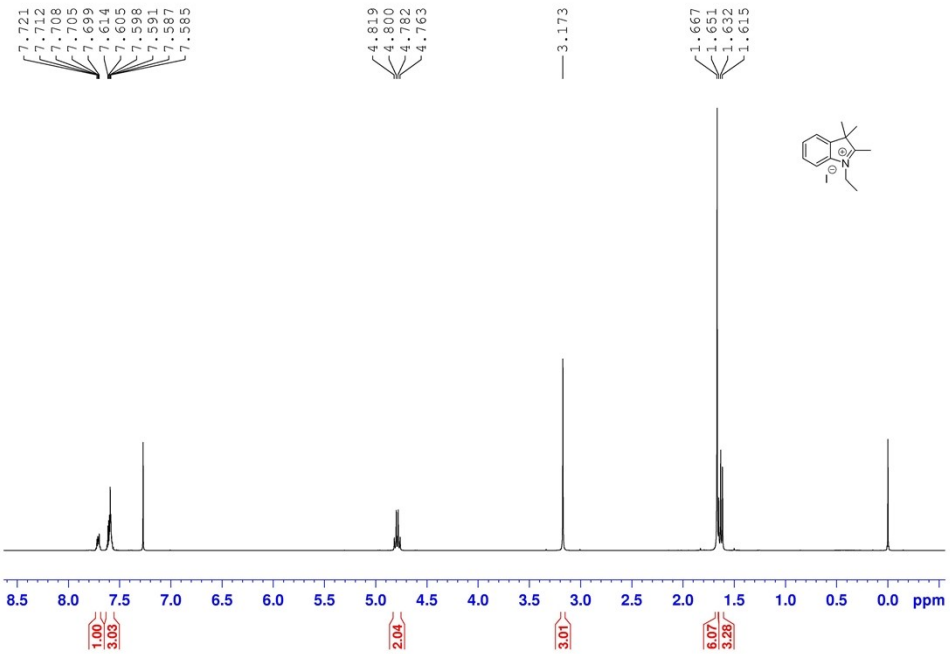

Figure S45. ^{1}H NMR spectrum of **Compound 4** in $CDCl_3$

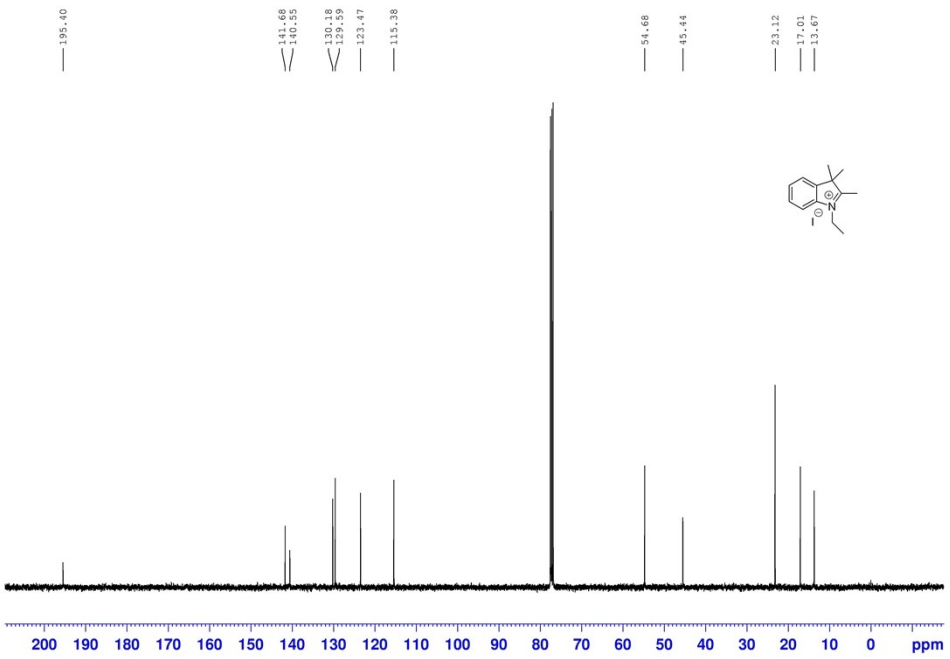

Figure S46. ^{13}C NMR spectrum of **Compound 4** in $CDCl_3$

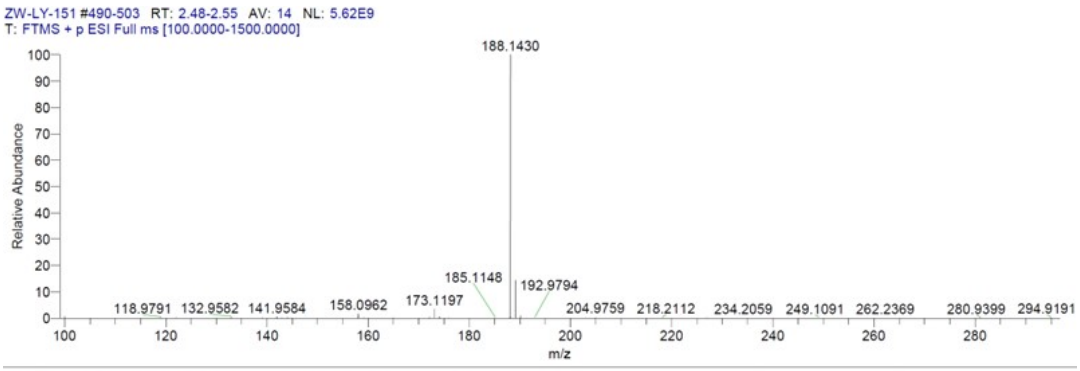

ZW-LY-151#491-506 RT: 2.49-2.56 AV: 16
T: FTMS + p ESI Full ms [100.0000-1500.0000]
m/z= 186.05-189.81

m/z	Intensity	Relative	Theo. Mass	Delta (ppm)	Composition
188.1430	5585867776.0	100.00	188.1434	-0.36	$C_{13}H_{18}N$

Figure S47. HRMS spectrum of **Compound 4**

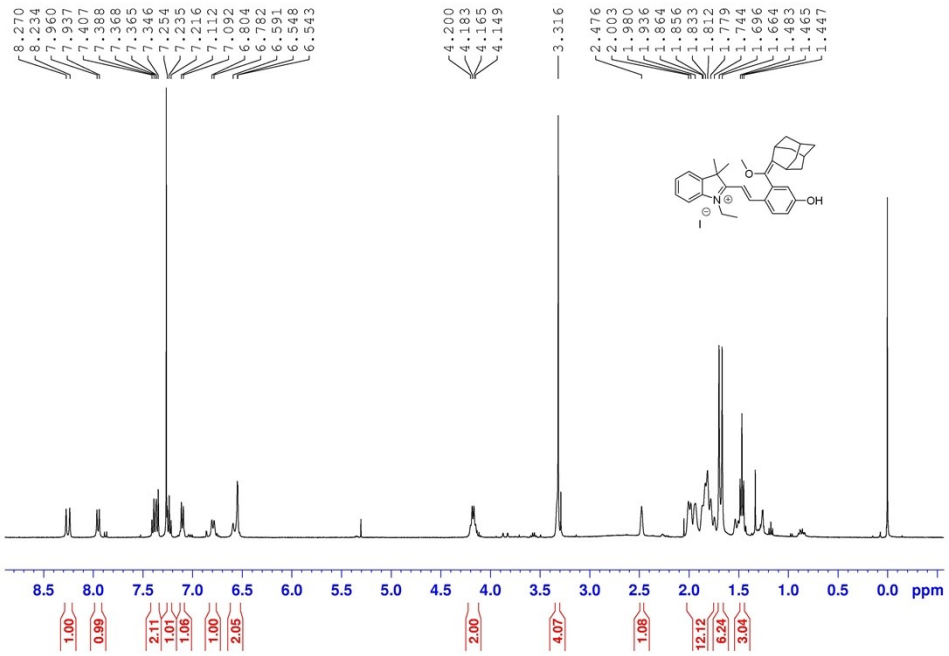

Figure S48. ^{1}H NMR spectrum of **InCL** in $CDCl_3$

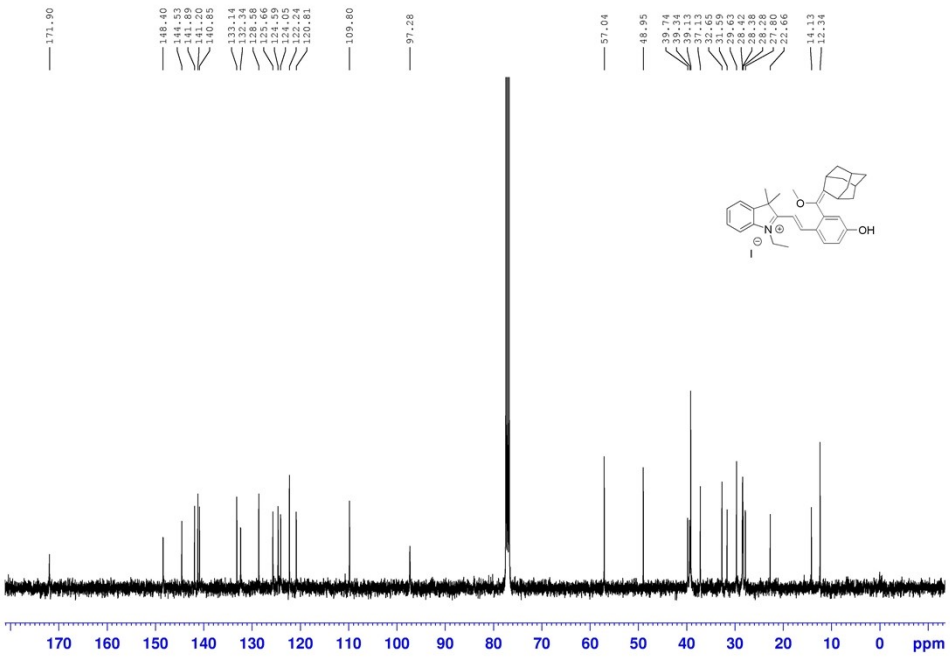

Figure S49. ^{13}C NMR spectrum of **InCL** in $CDCl_3$

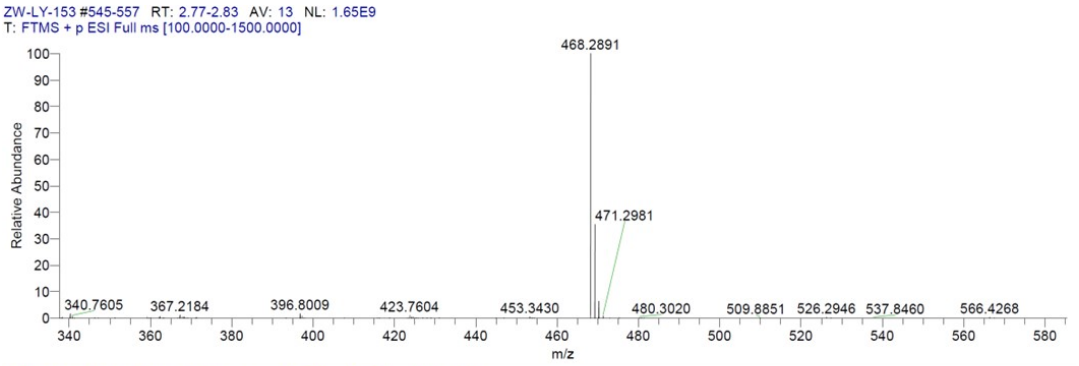

ZW-LY-153#544-561 RT: 2.76-2.85 AV: 18
T: FTMS + p ESI Full ms [100.0000-1500.0000]
m/z= 464.32-472.77

m/z	Intensity	Relative	Theo. Mass	Delta (ppm)	Composition
468.2891	1644930816.0	100.00	468.2897	-0.59	$C_{32}H_{38}O_2N$

Figure S50. HRMS spectrum of **InCL**

5. References

1. M. Liu, W. Zhai, H. Chen, H. Zhang and C. Li, *Anal. Chem.*, 2020, **92**, 10792-10799.
2. M. Frisch, G. Trucks; H. Schlegel, G. Scuseria, M. Robb, J. Cheeseman, G. Scalmani, V. Barone, G. Petersson, H. Nakatsuji, X. Li, M. Caricato, A. Marenich, J. Bloino, B. Janesko; R. Gomperts, B. Mennucci, H. Hratchian, J. Ortiz, A. Izmaylov, J. Sonnenberg, D. Williams, F. Ding, F. Lipparini, F. Egidi, J. Goings, B. Peng, A. Petrone, T. Henderson, D. Ranasinghe, V. Zakrzewski, J. Gao, N. Rega, G. Zheng, W. Liang, M. Hada, M. Ehara, K. Toyota, R. Fukuda, J. Hasegawa, M. Ishida, T. Nakajima, Y. Honda, O. Kitao, H. Nakai, T. Vreven, K. Throssell, Jr. Montgomery, J. Peralta, F. Ogliaro, M. Bearpark, J. Heyd, E. Brothers, K. Kudin, V. Staroverov, T. Keith, R. Kobayashi, J. Normand, K. Raghavachari, A. Rendell, J. Burant, S. Iyengar, J. Tomasi, M. Cossi, J. Millam, M. Klene, C. Adamo, R. Cammi, J. Ochterski, R. Martin, K. Morokuma, O. Farkas, J. Foresman and D. Fox, Gaussian 16, Wallingford, CT, 2016.
3. T. Yanai, D. P. Tew and N. C. Handy, *Chem. Phys. Lett.*, 2004, **393**, 51-57.
4. A. V. Marenich, C. J. Cramer and D. G. Truhlar, *J. Phys. Chem. B*, 2009, **113**, 6378-6396.
5. Y. Zhang, C. Yan, C. Wang, Z. Guo, X. Liu and W.-H. Zhu, *Angew. Chem., Int. Ed.*, 2020, **59**, 9059-9066.
6. T. Lu and F. Chen, *J. Comput. Chem.*, 2012, **33**, 580-592.
7. M. Yang, J. Zhang, D. Shabat, J. Fan and X. Peng, *ACS Sens.*, 2020, **5**, 3158-3164.